AtEH/Pan1 proteins drive phase separation of the TPLATE complex and clathrin polymerisation during plant endocytosis

Author list and affiliations

Jonathan Michael Dragwidge[1,2*], Yanning Wang[3], Lysiane Brocard[4], Andreas De Meyer[1,2], Roman Hudeček[5], Dominique Eeckhout[1,2], Clément Chambaud[6], Přemysl Pejchar[5], Martin Potocký[5], Michael Vandorpe[1,2], Amelie Bernard[6], Geert De Jaeger[1,2], Roman Pleskot[5], Xiaofeng Fang[3] and Daniël Van Damme[1,2*]

[1] Department of Plant Biotechnology and Bioinformatics, Ghent University, Technologiepark 71, 9052 Ghent, Belgium

[2] VIB Center for Plant Systems Biology, Technologiepark 71, 9052 Ghent, Belgium

[3] Center for Plant Biology, School of Life Sciences, Tsinghua University, Beijing, China

[4] Univ. Bordeaux, CNRS, INSERM, Bordeaux Imaging Center, BIC, UAR 3420, US 4, F-33000 Bordeaux, France

[5] Institute of Experimental Botany, Academy of Sciences of the Czech Republic, Rozvojová 263, 16502 Prague 6, Czech Republic

[6] Laboratoire de Biogenèse Membranaire, UMR 5200, CNRS, Univ. Bordeaux, F-33140 Villenave d'Ornon

*Corresponding author; email: jodra@psb.vib-ugent.be, dadam@psb.vib-ugent.be

Abstract

Endocytosis is the process by which cells internalise molecules from their cell surface via plasma membrane-derived vesicles. In plants, clathrin-mediated endocytosis requires the evolutionarily ancient TSET/TPLATE complex (TPC), which was lost in metazoan and fungal lineages. TPC is required for membrane bending, but how TPC functions in the initiation of endocytosis and clathrin assembly is unclear. Here we used live-cell imaging and biochemical approaches to investigate the function of the Arabidopsis thaliana TPC subunit AtEH1/Pan1. Using *in vitro* and *in vivo* experiments we found that AtEH/Pan1 proteins can self-assemble into condensates through phase separation, which is influenced by both structured and intrinsically disordered regions. The proteome composition of these condensates revealed many key endocytic components which are selectively recruited via prion-like- and IDR-based interactions, including the ESCRT-0 TOM-Like proteins. Furthermore, AtEH/Pan1 condensates selectively nucleate on the plasma membrane by binding specific phospholipid species that are recognised by their EH domains. Visualization of the ultrastructure of the endocytic condensates via CLEM-ET revealed that the coat protein clathrin can assemble into lattices within condensates. Our results reveal that AtEH/Pan1 proteins act as scaffolds to direct endocytic machinery to specific plasma membrane regions to initiate internalisation. These findings provide new insight into the interplay between membranes and protein condensates.

Introduction

Clathrin-mediated endocytosis is an essential process which allows cells to regulate the composition of their plasma membrane in response to external and internal stimuli. Clathrin-mediated endocytosis is a multi-step process involving nucleation, cargo recognition, clathrin recruitment, membrane invagination, vesicle scission and uncoating (Kaksonen and Roux, 2018; McMahon and Boucrot, 2011; Paez Valencia et al., 2016). The stages of nucleation and cargo recognition involve a complex network of transient interactions between early endocytic proteins, adaptor complexes, phospholipids, clathrin, and cargo molecules. Since core endocytic machinery was already present in the last eukaryotic ancestor (Field et al., 2007), the underlying principles which drive endocytosis appear largely conserved between eukaryotes from distinct super-kingdoms.

In humans, two of the earliest arriving endocytic proteins include the EH domain-containing protein Eps15 (Ede1p in yeast) (Stimpson et al., 2009; Taylor et al., 2011), and the muniscin proteins FCHo1/2 (Syp1p in yeast) (Henne et al., 2010). FCHo proteins interact with Eps15 via their µHD and bind the plasma membrane via interaction with anionic phospholipids (Alaoui et al., 2022; Day et al., 2021; Henne et al., 2010). This Eps15-FCHo1/2 module can activate the AP-2 adaptor complex to bind cargo (Hollopeter et al., 2014; Ma et al., 2015), leading to the recruitment of clathrin and further machinery to form clathrin coated pits (Cocucci et al., 2012). Consistently, depletion of Eps15 impairs endocytosis initiation (Bhave et al., 2020), while FCHo has additional roles in the stabilisation of endocytic pits (Bhave et al., 2020; Cocucci et al., 2012; Lehmann et al., 2019). How the initiator machinery collectively assembles on the membrane and recruits downstream endocytic components in a highly co-ordinated manner is still poorly understood.

Amoeba and plants contain an endocytic complex termed TSET and TPLATE complex (TPC) respectively. This complex is evolutionary ancient and related to COP and AP complexes (Gadeyne et al., 2014; Hirst et al., 2014; Yperman et al., 2021a; Zhang et al., 2015). In plants, TPC is essential, as mutants of TPLATE subunits cause male sterility (Gadeyne et al., 2014; Van Damme et al., 2006; Wang et al., 2019). TPC in plants functions in clathrin-mediated endocytosis together with AP-2 and is required for clathrin-curvature, as destabilisation of the complex causes a failure for clathrin pits to transition from a flat to a curved lattice (Gadeyne et al., 2014; Johnson et al., 2021; Wang et al., 2021). Compared to amoeba, plants contain two additional TSET subunits, AtEH1/Pan1 and AtEH2/Pan1, Eps15 homology (EH) domain containing proteins homologous to human Eps15 and yeast Ede1p and Pan1p. The evolutionarily conservation is highlighted by the conserved roles in autophagy between AtEH proteins (Wang et al., 2019), and Ede1p and Pan1p in yeast (Liu et al., 2022; Wilfling et al., 2020). AtEH1/Pan1 and AtEH2/Pan1 bind phospholipids and cargo through their EH domains (Yperman et al., 2021b), and dimerise via coiled-coiled domains (Sánchez-Rodríguez et al., 2018; Yperman et al., 2021a). Furthermore, AtEH1/Pan1 is structurally connected to TML via its lipid binding µ-homology domain (µHD) (Yperman et al., 2021a), placing both AtEH/Pan1 proteins and TML directly at the membrane surface. AtEH/Pan1 proteins are recruited to the PM simultaneously with the other TPC subunits (Wang et al., 2020), but how they function together with the other TPC subunits to facilitate clathrin-mediated endocytosis is still unclear.

Recently, the formation of membraneless organelles (or biomolecular condensates), which are assembled through liquid-liquid phase separation, emerged as a fundamental mechanism to compartmentalise cellular functions (Banani et al., 2017; Choi et al., 2020; Snead and Gladfelter, 2019;

Zhao and Zhang, 2020). These include processes where condensates form on the surface of membranes, including autophagosome assembly (Fujioka et al., 2020), tight-junction formation (Beutel et al., 2019), and endocytosis (Bergeron-Sandoval et al., 2021; Day et al., 2021). In humans, Eps15 and Fcho1/2 phase separate to delineate membrane domains and catalyse the early formation of clathrin coated pits (Day et al., 2021). We hypothesised that in plants AtEH/Pan1 proteins may function as part of a similar initiator module to drive the efficient initiation and stabilisation of endocytosis via phase separation.

Here we performed live-cell imaging, electron-tomography, interactomics, and *in vitro* biochemical experiments to decipher the function of the AtEH/Pan1 proteins. We found that AtEH/Pan1 can form condensates through phase separation, which recruits various endocytic accessory proteins, including clathrin. The nucleation of these condensates requires lipid binding on the plasma membrane and these condensates form a platform for clathrin recruitment and polymerization. Our results reveal that AtEH/Pan1 proteins act as endocytic scaffolds through the formation of membrane bound condensates which underlies the initiation and progression of endocytosis.

Results

AtEH/Pan1 proteins undergo liquid-liquid phase separation

AtEH1/Pan1 and AtEH2/Pan1 are plant-specific subunits of TPC that are connected to the other six subunits via a physical interaction with the TML subunit (Yperman et al., 2021a) (Fig. 1A). AtEH/Pan1 subunits have a similar domain architecture (Fig. 1B), and are proposed to have homologous, but non redundant functions during endocytosis (Gadeyne et al., 2014; Wang et al., 2019). Sequence analysis indicates that AtEH1/Pan1 and AtEH2/Pan1 are proportionally much more disordered than the other TPC subunits (Fig S1A-B), containing multiple long stretches of disordered residues (Fig. 1B). Furthermore, AtEH/Pan1 proteins contain prion-like domains (PrLDs) in their N-terminal intrinsically disordered regions (IDRs) (Fig. 1B). Prion-like domains and long IDRs are a common feature of proteins which undergo phase separation and form biomolecular condensates in cells (Alberti et al., 2019). As AtEH/Pan1 homologs from yeast (Ede1) and humans (Eps15) have the ability to undergo phase separation (Day et al., 2021; Kozak and Kaksonen, 2019; Wilfling et al., 2020), we asked whether this may be an evolutionarily conserved property of these proteins.

Transient overexpression of AtEH/Pan1 proteins in tobacco (*Nicotiana benthamiana*), or overexpression in *Arabidopsis thaliana* seedlings were previously shown to form punctate structures (Wang et al., 2019), (Fig. 1C-D). Similar structures were observed by overexpression of AtEH1/Pan1 in fission yeast (*Schizosaccharomyces pombe*) (Fig 1E). Overexpression of other TPC subunits does not result in similar structures in *N. benthamiana* (Wang et al., 2019; Yperman et al., 2021a). We next assessed whether these structures have biophysical properties consistent with condensates. Under very high expression levels achieved using an Estradiol inducible promoter in *A. thaliana*, puncta showed rapid growth and shedding consistent with Ostwald ripening (Fig. 1F), and fused with each other (Fig. 1G). Latrunculin B abolished the mobility of these puncta, indicating that they move on actin (Fig. S2A), which is in agreement with AtEH/Pan1 proteins binding directly to actin *in vitro* (Wang et al 2019). Fluorescence recovery after photobleaching (FRAP) experiments indicate that AtEH1/Pan1-GFP molecules are rapidly exchanged between the condensate and the cytosolic pool

(Fig. 1H). Fast recovery, fusion, and rapid growth and dissolution of these condensates is consistent with the properties of proteins that phase separate.

Multiple domains of AtEH1/Pan1 contribute to its phase separation behaviour

Protein phase separation can be driven by intra- and inter-molecular multivalent interactions, for example by interaction between structured domains, or through weak interactions mediated by individual residues in IDRs. To assess which domains of AtEH/Pan1 proteins facilitate phase separation, we performed phase separation assays *in vitro* and *in vivo*, focusing on AtEH1/Pan1 due to its more central connection to TML and TPLATE in TPC when compared to AtEH2/Pan1 (Yperman et al., 2021a).

We generated three AtEH1/Pan1 constructs; full length ($AtEH1_{FL}$), an IDR3 truncation ($AtEH1_{1-684}$), and a coiled-coil and IDR3 truncation ($AtEH1_{1-527}$), and fused them with MBP-TEV-GFP at their N-terminus (Fig. 2A). We expressed and purified these proteins recombinantly in *E. coli* and performed *in vitro* phase separation assays (Fig. 2B-C). Full length AtEH1/Pan1 phase separated at relatively low protein concentrations (≤ 0.1 µM) consistent with strong phase separation observed *in vivo* (Fig. 2C-D). Furthermore, phase separation of AtEH1/Pan1 was salt-independent, and at high concentrations the protein partially aggregated (≥ 2.5 µM). Fluorescence recovery within *in vitro* AtEH1/Pan1 condensates was low (Fig 2E). This may suggest that intra-molecular interactions promote phase separation and limit molecular re-arrangement in the absence of other components. Phase separation *in vitro* was drastically reduced when the intrinsically disordered C-terminus (IDR3) was truncated, and abolished when the coiled-coil domain was further truncated (Fig 2D), indicating that these regions are important for phase separation of AtEH1/Pan1 in the absence of other factors.

Next, we generated AtEH1/Pan1-GFP truncation constructs and assessed their ability to phase separate *in planta,* via transient expression in *N. benthamiana*, and heterologously, by stable integration in *S. pombe* (Fig. 2F-G, S3). Deletion of IDR3 ($AtEH1_{1-684}$), and truncation (or deletion) of the coiled-coil domain ($AtEH1_{1-527}$, $AtEH1/_{\Delta CC}$) significantly reduced, but did not abolish condensate formation *in planta*. Deletion of IDR3 alone abolished actin-dependent motility (Fig. S2B). Truncation of the first EH domain ($AtEH1_{125-1019}$), or subsequent IDR1 ($AtEH1_{302-1019}$), drastically increased the phase separation threshold, indicating that this N-terminal region is important for driving phase separation *in planta*. However, in yeast, truncation of the entire N-terminus did not abolish phase separation ($AtEH1_{528-1019}$). The differential behaviour of these proteins in the different cellular contexts suggests that phase separation regulation in plants may depend on additional components that are absent in yeast or that phase separation in yeast is enhanced based on yeast-specific components or expression levels.

Since IDR1 appeared to have a large effect in determining phase separation *in vivo*, we assessed whether specific residues in this region hold a critical function. Sequence alignment of AtEH/Pan1 homologs throughout 700 million years of evolution indicated that while IDR1 was relatively divergent at a single amino acid level (Fig. S4A), the relative proportion of amino acid classes was highly conserved (Fig. S5). Phase separation can be driven by charge or hydrophobic interactions mediated by various residues (e.g.: π–π interactions via aromatic residues) (Boeynaems et al., 2018). To test whether specific residues were critical for phase separation we mutated aromatic, charged, and proline residues, but did not observe an abolishment of the condensate forming capacity of these proteins (Fig. S4B). Increasing aromatic interaction strength by exchanging tyrosine and phenylalanine

residues for tryptophan (12YF>W) caused aberrant condensate formation, which displayed increased solidity as revealed by live-cell imaging (Fig. S4C). Altogether, our findings suggest that while IDR1 can influence the physical properties of the condensates, the formation, or nucleation of the condensates occurs through mechanisms independent of weak interactions mediated by IDR1.

AtEH/Pan1 condensates nucleate by lipid binding on the plasma membrane

The nucleation or assembly of condensates is not spontaneous, and requires overcoming an energy barrier before molecular interactions reach a critical threshold for phase separation (Martin et al., 2021). Since AtEH1/Pan1 is recruited to the plasma membrane during early endocytosis together with other TPLATE subunits (Wang et al., 2020), we reasoned that the plasma membrane could act as a condensate nucleation surface. To test this, we performed live-cell imaging of AtEH1/Pan1-GFP in *N. benthamiana* epidermal cells. We observed simultaneous nucleation events on the surface of the plasma membrane, with condensates gradually increasing in size before dissociating from the membrane (Fig. 3A). These nucleation events were much slower than endocytic events, lasting approximately 100 seconds. Furthermore, without its C-terminal region required for actin binding, AtEH1/Pan1 formed immobile, regularly spaced condensates on the surface of the membrane (Fig. 3B, S2B). These data suggest that AtEH/Pan1 proteins may directly bind components of the plasma membrane resulting in their recruitment, concentration and subsequently nucleation of phase separation.

As AtEH/Pan1 subunits can bind negatively charged phospholipids via their EH domains (Yperman et al., 2021b), we questioned whether AtEH1/Pan1 condensates could be initiated by the binding of AtEH/Pan1 to anionic phospholipids in the plasma membrane. To test this, we mutated 3 positively charged arginine or lysine residues which mediate lipid binding in each individual EH domain (Yperman et al., 2021b), and examined the effect on condensate formation in *N. benthamiana*. Disrupting lipid binding capacities of individual EH domains significantly increased the saturation concentration required for phase separation for both full length and truncation constructs (Fig. 3C-D), and often lead to the formation of irregularly shaped, or abnormally large condensates in the cell. Mutation of both EH domains' capacity to bind lipids completely abolished phase separation (Fig. 3C-D), demonstrating that lipids are the primary interaction partner of AtEH/Pan1 subunits to facilitate condensate nucleation. However, we did observe partial phase separation even after mutation of both EH domains using an AtEH1/Pan1 construct lacking the C-term ($AtEH1_{1-684}$), suggesting that under certain conditions, which are mimicked here by truncating the C-term, additional binding partners present in the N-terminal region may act as secondary interactors of AtEH/Pan1 proteins at the membrane to facilitate condensate nucleation.

The plasma membrane in plants is composed of multiple lipid species, including the phospholipids phosphatidic acid (PA), phosphatidylinositol 4-phosphate (PI4P), and phosphatidylinositol 4,5-bisphosphate ($PI(4,5)P_2$) (Noack and Jaillais, 2017; Noack and Jaillais, 2020). To determine whether specific lipids are required for the nucleation of AtEH/Pan1 condensates, we examined condensate formation by transient overexpression of AtEH1/Pan1 in *Nicotiana tabacum* pollen tubes, which maintain a strict and distinctive lipid composition at different plasma membrane regions (Potocký et al., 2014a). We found that AtEH1/Pan1 preferentially formed condensates at the sub-apical region of growing pollen tubes which co-localised strongly with PA and PI4P biosensors, but not PI(4,5)P2 (Fig. 3E). These findings are consistent with our previous report that both EH domains strongly bind PA

(Yperman et al., 2021b). We therefore conclude that AtEH1/Pan1 likely nucleates by recognition of PA on the plasma membrane. Furthermore, under endogenous expression levels TPC components TPLATE and TML show similar localisation patterns (Gadeyne et al., 2014; Van Damme et al., 2006), indicating that the TPC is driven to the membrane via the lipid binding activity of AtEH/Pan1 subunits.

AtEH1/Pan1 functions as a scaffold to recruit endocytic accessory proteins

Condensate formation can be driven by highly multivalent proteins (termed scaffolds) which can passively recruit lower valency proteins (termed clients) into condensates (Banani et al., 2016). We therefore asked whether AtEH/Pan1 proteins could act as a scaffold and recruit endocytic proteins into the condensate. To identify putative client proteins, we performed proximity labelling proteomics in *A. thaliana* cell culture using AtEH1/Pan1-TurboID as a bait (Fig. 4A). Because this system expresses the bait proteins in the presence of the endogenous genes, and AtEH1/Pan1 can phase separate by itself when overexpressed, we compared AtEH1/Pan1-TurboID data with available data from another TPLATE complex subunit (TPLATE-TurboID) to discriminate between endocytic interactors and interactions due to overexpression of AtEH1/Pan1 (Arora et al., 2020).

TOM-1LIKE (TOL) proteins TOL6 and TOL9, members of an ancestral ESCRT-0 complex which localize at the plasma membrane and function as ubiquitin receptors in plants were common between both baits (Fig. 4B) (Blanc et al., 2009; Herman et al., 2011; Korbei et al., 2013; Moulinier-Anzola et al., 2020). Furthermore, we found late stage endocytic proteins, including dynamins (DRP1B, DRP2A, DRP2B) which mediate vesicle scission (Fujimoto et al., 2010; Konopka and Bednarek, 2008), and AUXILIN-LIKE proteins, which function in vesicle uncoating (Adamowski et al., 2018). Sequence analysis indicated that TOL6 and TOL9 contain large prion-like domains (Fig. S6A-B), while AUXILIN-LIKE and DRP2 proteins contained large, disordered regions. We hypothesized that these structural features could potentially mediate weak-multivalent interactions with AtEH1/Pan1, and therefore be recruited into AtEH1/Pan1 condensates.

To test this, we performed a phase separation partitioning assay by expressing AtEH1/Pan1 (scaffold) with the identified client proteins in *N. benthamiana*. We observed that TOL6 and AUXILIN-LIKE 1 readily partitioned into AtEH1/Pan1 condensates and that this was independent of the C-terminus of AtEH1/Pan1. However, interaction with TOL6 was significantly increased in the AtEH1/Pan1$_{1\text{-}684}$ background (Fig. 4C), likely as TOLs remain membrane bound and do not completely partition into condensates (Fig. S6C). Lastly, DRP2a partitioned into AtEH1/Pan1$_{FL}$, but not into AtEH1/Pan1$_{1\text{-}684}$ condensates, suggesting that the C-terminus mediates the interaction here. We purified TOL6 and TOL9 and performed partitioning assays *in vitro* (Fig. 4E). Despite containing relatively large prion-like domains and high disorder content, TOL6 and TOL9 did not undergo phase separation alone (Fig. 4E) (Fig. S6A-B). When combined with AtEH1/Pan1, TOL6 and TOL9 partitioned into the condensates (Fig. 4E). These data show that AtEH1/Pan1 is a scaffold which drives the recruitment of endocytic proteins into condensates.

Next, we asked if we could identify sequence features of proteins that would specify their interaction with AtEH1/Pan1. When we assessed the individual datasets, we found that the AtEH1/Pan1-TurboID dataset was highly enriched in disordered and prion-like domain containing proteins when compared to TPLATE-TurboID (Fig. S6A-B, D). These included many prion-like domain containing cytosolic and nuclear proteins which are implicated in phase separation (Cho et al., 2018; Fang et al., 2019). We

reasoned that these proteins may be recruited to cytosolic condensates caused by overexpression of AtEH1/Pan1, which we confirmed by partitioning in *N. benthamiana* (Fig. S6E). We then assessed the composition of these prion-like domains compared to with those from the *A. thaliana* proteome (Chakrabortee et al., 2016; Powers et al., 2019), and found that prion-like domains enriched in AtEH1/Pan1-TurboID are enriched in glutamine (Fig. 4F), remarkably similar to the composition of TOL6 and TOL9 prion-like domains. These findings indicate that AtEH1/Pan1 condensates preferentially recruit prion-like proteins with specific properties. Collectively, our data demonstrate that AtEH1/Pan1 proteins recruit endocytic proteins through IDR-based interactions.

Clathrin forms cage-like assemblies at AtEH1/Pan1 condensates

To understand the morphology of AtEH1/Pan1 condensates, we performed correlative light and electron microscopy (CLEM) combined with electron tomography (ET) in 35S::AtEH1/Pan1-GFP overexpression lines (Fig. 5A). Remarkably, we resolved that AtEH1/Pan1 condensates contained structured polygonal cage-like assemblies, which appeared to be arranged on the condensate surface (Fig. 5A). We did not observe membranes in these structures, indicating that they are condensates and not membrane bound clathrin-coated assemblies. The dimensions and arrangement of these assemblies closely match the dimensions of higher order polygonal structures formed by the coat protein clathrin (Morris et al., 2019). To confirm that these structures were clathrin, we examined the localisation of clathrin light chain (CLC2) in 35S::AtEH1/Pan1-GFP lines. We found that, similar to what has been shown in *N. benthamiana* (Wang et al., 2019), clathrin also partitioned with AtEH1/Pan1 in Arabidopsis, and in some cases clathrin accumulated around the condensates (Fig. 5B). These findings indicate that AtEH1/Pan1 condensates recruit and concentrate clathrin, which can then assemble into organised coat structures.

Discussion

AtEH/Pan1 proteins are endocytic scaffolds

Our *in vitro* and *in vivo* data shows that AtEH/Pan1 proteins can phase separate and recruit endocytic proteins, and therefore likely act as key scaffold proteins during endocytosis. This is supported by analysis of the domain architecture of AtEH/Pan1 subunits, which is remarkably similar to other essential scaffold proteins which drive the formation of diverse condensates in cells, such as the stress granule scaffold G3BP (Yang et al., 2020). These proteins are characterised by an oligomerisation domain, an intrinsically disordered region, and a substrate binding domain (Mitrea and Kriwacki, 2016; Sanders et al., 2020). We show that the coiled-coil domain of AtEH1/Pan1 promotes phase separation *in vitro* and in plant cells, and therefore functions as an oligomerisation domain, similar to the coiled-coil domains in AtEH/Pan1 homologs Eps15 and Ede1 (Boeke et al., 2014; Lu and Drubin, 2017; Tebar et al., 1997). Furthermore, the intrinsically disordered, prion-like regions in the N-terminus controls the material properties of endocytic condensates. Lastly, the C-terminal IDR acts as the primary substrate binding domain, facilitating multiple protein-protein interactions including dynamin (during endocytosis), and ARP3 and VAP27-3 (during autophagy) (Wang et al., 2019).

It is evident that AtEH/Pan1 proteins function in endocytosis and in autophagy (Gadeyne et al., 2014; Stephani et al., 2020; Wang et al., 2019; Wang et al., 2020). This is also supported by the findings from

Wilfling et al., 2020, who show that in yeast Ede1 acts as an intrinsic autophagy receptor to degrade aberrant endocytic structures. While it was previously proposed that AtEH/Pan1 condensates in *N. benthamiana* were autophagosomes based on co-localisation with ATG proteins (Wang et al., 2019), we find that in this system, these structures are instead condensates which are likely degraded through autophagy. It is unclear how AtEH/Pan1-mediated endocytosis and autophagy processes are functionally segregated, but this could involve conformational changes or post-translational modifications which modify the accessibility of protein-interaction sites. This may also explain how recruitment of dynamin and Auxilin-like proteins could be regulated, as they partition into AtEH1/Pan1 condensates but only function during later endocytic stages of scission and uncoating respectively (Adamowski et al., 2018; Fujimoto et al., 2010).

Given that AtEH/Pan1 are structurally and functionally similar to yeast Ede1 and human Eps15 which can form condensates (Day et al., 2021; Kozak and Kaksonen, 2019; Wilfling et al., 2020), and have been proposed to function as early endocytic scaffolds (Maldonado-Báez et al., 2008; McMahon and Boucrot, 2011), we propose that AtEH/Pan1 may have evolved from an ancient scaffold protein which function in endocytic initiation and progression.

AtEH/Pan1 subunits are condensate nucleation machinery which initiate endocytosis at the membrane

Endocytosis functions to selectively internalise portions of the plasma membrane. How endocytosis is initiated in plants is unclear, but is proposed to involve the assembly of a nucleation module before activation of AP-2 and the arrival of TPC before clathrin (Gadeyne et al., 2014; Narasimhan et al., 2020; Paez Valencia et al., 2016). Our data suggests that in plants, this selectivity may be achieved by the targeting of AtEH/Pan1 proteins to lipid domains in the plasma membrane enriched for PA and PI4P. This is consistent with previous findings that AtEH/Pan1 subunits bind phospholipids via their EH domains and can localise to the cell plate (Yperman et al., 2021b), which is enriched in PA and PI4P (Noack and Jaillais, 2020; Platre et al., 2018). Furthermore, AtEH1/Pan1 remains at the plasma membrane when the TPC subunit TPLATE is forced to aggregate in the cytoplasm (Wang et al., 2021). Furthermore, TML can bind PI4P at the plasma membrane via its muniscin homology domain (μHD), which is structurally connected to AtEH1/Pan1 (Fig 1A) (Yperman et al., 2021a), and may provide additional specificity or affinity to stabilise the entire TPLATE complex on the target membrane.

In animal cells endocytosis is initiated by the AtEH/Pan1 and TML homologs Eps15 and FCHo1/2 respectively, which function in the initiation and stabilisation of clathrin coated vesicles (Bhave et al., 2020; Day et al., 2021; Henne et al., 2010; Lehmann et al., 2019). In plants, AtEH/Pan1 are recruited simultaneously with other TPC subunits and remain present during all observable stages of endocytosis (Gadeyne et al., 2014; Wang et al., 2020). Therefore, the recruitment of the whole TPLATE complex to lipid domains of the plasma membrane would be sufficient to overcome a phase separation threshold (Snead and Gladfelter, 2019), leading to condensate formation and the recruitment of endocytic accessory proteins and clathrin, and therefore the progression of endocytosis. Because arrival of TPC precedes clathrin at endocytic sites (Gadeyne et al., 2014; Narasimhan et al., 2020), condensate formation could precede clathrin assembly and polymerisation, and that clathrin assembles in a liquid-like state with other endocytic accessory proteins (Fig. 5). How clathrin interacts with or assembles with endocytic condensates is not clear, but it may be due to TPC

subunits such as TPLATE, containing uncharacterised clathrin interaction motifs (Gadeyne et al., 2014; Van Damme et al., 2011).

In contrast to full length AtEH/Pan1 where both EH domains were mutated to abolish lipid binding, we still observed condensate formation with AtEH1/Pan1, lacking lipid binding capacity as well as lacking the C-term. Binding of the N-terminus of AtEH/Pan1 subunits to other plasma membrane components may therefore substitute for lipid-dependent membrane recruitment. We previously identified TOM-like proteins as putative interactors of the TPLATE complex (Arora et al., 2020), and here show that AtEH1/Pan1 can recruit TOL6 into membrane bound condensates, likely via interaction of glutamine rich prion domains which are specifically enriched in AtEH1/Pan1 condensates. Because TOLs function as ubiquitin receptors as part of the heteromeric ESCRT-0 complex in plants (Korbei et al., 2013; Moulinier-Anzola et al., 2020), co-operative binding to TOLs may provide additional cues to specifically target AtEH/Pan1 proteins (and therefore TPC) to membrane regions enriched for cargo primed for internalisation. Interestingly, Eps15 interacts with the human ESCRT-0 component hepatocyte growth factor-regulated tyrosine kinase substrate (HRS) (Bache et al., 2003), suggesting that a link between ESCRT-0, AtEH/Pan1 proteins, and endocytosis initiation may be evolutionarily conserved. AtEH/Pan1 proteins can also interact with proteins containing NPF motifs via their EH domains (Yperman et al., 2021b), and therefore NPF-containing PM proteins such as Secretory Carrier Membrane Protein 5 (SCAMP 5) cannot be excluded as additional weak recruitment signals in addition to TOLs.

Glutamine rich prion-like domains are a conserved sequence feature of endocytic proteins in yeast (Bergeron-Sandoval et al., 2021), suggesting that the biophysical properties of condensates may be similar. Further analysis of how the composition and sequence variability of IDRs of AtEH/Pan1 proteins influence the properties and composition of endocytic condensates warrants further investigation. IDR mediated interactions could be facilitated by both linear binding motifs of motif-independent interactions encoded by sequence chemistry (Langstein-Skora et al., 2022), for example by linear binding motifs present on the C-terminus of AtEH1/Pan1 which may encode for recruitment of dynamin (DRP2a), while motif-independent interactions may drive the recruitment of TOL proteins.

Conclusions

The endocytic site is composed of a meshwork of dozens of interacting proteins which are dynamically re-modelled during the formation of clathrin coated pits (Schmid and McMahon, 2007). Weak, multivalent interactions, which can be dynamically re-arranged, are a common property of phase separated biological systems (Banani et al., 2017; Ditlev et al., 2018). Consistently, clathrin and certain endocytic proteins are rapidly exchanged during clathrin-coated pit formation (Avinoam et al., 2015; Bergeron-Sandoval et al., 2021; Skruzny et al., 2020). The liquid-like properties of endocytic condensates may provide an ideal environment for both the recruitment and re-arrangement of proteins during endocytic progression. Artificially strengthening condensate interactions during early clathrin coated pit formation stalls endocytosis (Day et al., 2021), suggesting that the material properties of these condensates are critical for their function. Further meso-scale understanding of the properties of these condensates and how they are regulated will be essential to understanding their function.

Collectively, our data shows that AtEH/Pan1 subunits of the endocytic TPLATE complex can phase separate to form endocytic condensates and that the nucleation of the phase separation occurs on the membrane. We propose that AtEH/Pan1 are key scaffolds that initiate endocytosis at the plasma membrane through lipid binding, leading to the efficient recruitment of other TPC subunits, monomeric adaptors, clathrin, AP-2, but also TOL proteins, to the growing clathrin coated pit. This work provides new mechanistic insight into how plants internalise cargo proteins.

Acknowledgements

We thank Evelien Mylle and Matthieu Buridan for technical support. Work in the D.V.D lab is supported by the European Research Council Consolidator ERC grant (T-REX; 682436). J.MD. is supported by a Research Foundation–Flanders (FWO) postdoctoral fellowship (12S7222N), and an EMBO Scientific exchange grant (#9253). A.M.D is supported by an FWO PhD Fellowship grant. R.P. is supported by the Czech Science Foundation grant nr. 22-35680M. C.C. and A.B are supported by the European Research Council under the European Union's Horizon 2020 research and innovation programme (grant agreement No 852136 to A.B.).

Author contributions

J.M.D initiated the project, designed and performed all experiments unless otherwise indicated, under supervision of D.V.D. Y.W. purified proteins, performed in-vitro assays and yeast localisation under supervision of X.F. L.B. and J.M.D designed and performed the CLEM-ET experiments. C.C. assisted with CLEM-ET experiments and analysis under supervision of A.B. A.D.M. performed partitioning assays in tobacco. R.H., R.P. and M.P. performed the pollen tube experiments. R.P. made the EH sequence alignment and phylogenetic tree. M.V. and P.P. cloned constructs. D.E. performed proteomics analysis under supervision of G.D.J. J.M.D and D.V.D wrote the manuscript. All authors contributed to finalising the text.

Materials and Methods

Plant material and growth conditions

A. thaliana lines were all in the Columbia-0 (Col-0) accession background. Plant lines have been previously described; 35S::AtEH1/Pan1-GFP, pRPS5A::XVE:AtEH1/Pan1-GFP, pRPS5A::XVE:AtEH2/Pan1-GFP (Wang et al., 2019), CLC2-mKO (Ito et al., 2012).

Seeds were surface sterilised by chlorine gas and grown on ½ strength Murashige and Skoog (½ MS) medium containing 0.6% (w/v) agar pH 5.8, without sucrose. Seedlings were stratified for 48 h at 4°C in the dark, and transferred to continuous light conditions (68 µE m−2 s−1 photosynthetically active radiation) at 21 °C in a growth chamber. Imaging was performed on 4-5 day old seedlings unless otherwise indicated. β-Estradiol induction of the pRPS5A::XVE lines was performed by transferring 3-day-old seedlings to ½ MS medium containing 1 µM β-estradiol (Sigma-Aldrich).

Molecular cloning

To generate the constructs used for heterologous expression in yeast cells, AtEH1/Pan1 and its variants coding sequences were amplified and cloned into pDUAL-Pnmt1-yeGFP vector by the ClonExpress II One Step Cloning Kit (Vazyme, C112).

The constructs for *in vitro* protein expression were cloned by inserting AtEH1(FL), AtEH1(1-684) and AtEH1(1-527) coding sequences into MBP-HIS-GFP vector, with maltose binding protein (MBP) at N-terminus following a TEV cleavage site and a green fluorescence protein (GFP) at C-terminus. The sequences of TOL6 and TOL9 were amplified and inserted into the pRSFduet-6×His-mCherry vector to generate mCherry-TOL6 and mCherry-TOL9 constructs for in vitro protein expression.

To prepare the PA marker construct (pLat52::mRFP:NES-2xSpo20p-PABD), NES-Spo20p-PABD was first amplified using P1 and P2 primers and YFP:Spo20p-PABD (Potocký et al., 2014b) as a template and introduced into mRFP:2xSpo20p-PABD (Pejchar et al., 2020) using XbaI/SpeI sites to make mRFP:NES-2xSpo20p-PABD. To prepare the PI4P marker construct (pLat52::mRFP:2xP4M-SidM), 2xP4M-SidM was first amplified using P3 and P4 primers and GFP:P4M-SidM2x (a gift from Prof. Tamas Balla, Addgene plasmid # 51472) as a template and introduced into the vector pHD22, kindly provided by Prof. Benedikt Kost, using XbaI/ApaI sites to make mRFP:2xP4M-SidM. Construct for PI(4,5)P2 marker, mRFP:2xPHPLCδ1, was described previously (Scholz et al., 2022).

All other constructs were cloned using the green gate system (Lampropoulos et al., 2013), and are detailed in Table S1.

TurboID

PSB-D *A. thaliana* cell suspension cultures were transformed with the AtEH1/Pan1-linker-TurboID and experiments were performed as previously described (Arora et al., 2020). The TPLATE-linker-TurboID dataset is described before (Arora et al., 2020). To calculate enrichment scores, the datasets were compared to a large set of TurboID experiments using unrelated baits performed using the same conditions.

CLEM-ET

The CLEM approach was performed similarly to previously described with minor modifications (Chambaud et al., 2022). Hypocotyls of 4-day old *A. thaliana* seedlings stably expressing 35S:AtEH1-GFP were cut and frozen in a Leica EM-PACT high-pressure freezer using 20% BSA as a cryoprotectant. Freeze-substitution was performed using a Leica AFS 2 using 0.1% uranyl acetate. Hypocotyls were embedded in HM20 Lowicryl resin (Electron Microscopy Science). Ultra-thin sections were cut using a microtome (Leica Ultracut) with a diamond knife (Biel, Switzerland) and placed on copper mesh grids (Electron Microscopy Science). Sections were treated with Anti-GFP primary antibody and 5 nm gold conjugated secondary antibody to assist in the correlation of fluorescence signal due to limited landmarks in hypocotyl samples.

EM grids were imaged before ET by fluorescence microscopy using a Zeiss LSM 880 Airyscan confocal microscope with a 63× apochromatic N.A 1.4 oil objective. Transmission electron microscopy observations were carried out on a FEI TECNAI Spirit 120 kV electron microscope equipped with an Eagle 4Kx4K CCD camera. Electron tomography was performed as previously described (Nicolas et al., 2018). Tilt series were acquired from -65° to 65°. To acquire dual axis tomograms the grid was rotated 90°. The raw tilt series were aligned and then reconstructed using the fiducial alignment mode with the eTomo software (http://bio3d.colorado.edu/imod/). 10 to 25 fiducials were used to accurately align all images. Reconstruction was performed using the back-projection with SIRT-like filter (10 to 50 iterations).

Transient expression in Tobacco

N. benthamiana plants were grown in a greenhouse under long-day conditions (6–22 h light, 100 PAR, 21 °C) in soil (Saniflor osmocote pro NPK: 16-11-10 + magnesium and trace elements). Transient expression was performed by leaf infiltration according to (Sparkes et al., 2006). A similar optical density of Agrobacterium strains was used for all constructs during co-expression. Transiently transformed *N. benthamiana* were imaged three to four days after infiltration.

Confocal microscopy

Spinning Disk: Imaging was performed on a PerkinElmer Ultraview spinning-disc system, attached to a Nikon Ti inverted microscope, and operated using the Volocity software package. Images were acquired on an ImagEM CCD camera (Hamamatsu C9100-13) using frame-sequential imaging with a 60x water immersion objective (NA = 1.20). Specific excitation and emission were performed using a 488 nm laser combined with a single band pass filter (500-550 nm) for GFP in single camera mode. RFP was visualized using 561 nm laser excitation and a 570-625 nm band pass filter. Exposure time was between 25-500 ms.

Image Analysis: For FRAP, fusion, and ostwald ripening experiments condensates were tracked using Trackmate (Tinevez et al., 2017). Relative fluorescence intensity profiles were obtained and plotted.

For the analysis of AtEH1/Pan1 truncations or mutations in tobacco the relative saturation concentration was obtained by quantifying the mean cytosolic signal after subtraction of background signal. The partitioning assay quantification was performed using the MitoTally script using regions of interests determined from AtEH1/Pan1 positive foci (Winkler et al., 2021).

Fluorescence recovery after photobleaching (FRAP)

Tobacco cells transiently expressing proteins were inhibited with Latrunculin B (4 µM) for 30 minutes prior to imaging to inhibit condensate movement. FRAP was performed on the spinning disk system using the Ultraview PhotoKinesis unit. Bleaching was performed with 100% 488 laser for 3s and post-bleach acquisition was performed every 0.6 seconds for 120 seconds. Analysis was performed using easyFRAP (Rapsomaniki et al., 2012).

For the FRAP experiments *in vitro*, MBP-EH1(FL)-GFP was cleaved with TEV protease for 3 hours to remove MBP tag. EH1-FL protein was diluted into 10 µM at 100 mM NaCl. After 30 min of incubation on ice, droplets were bleached with a 488-nm laser pulse (3 repeat, 100% intensity) on Zeiss LSM880 confocal laser microscope using a ×63 objective. Fluorescence recovery was recorded every 2 s for 400 s after bleaching. Images were acquired using ZEN software. Using Fiji/ImageJ to analyse the fluorescence intensity of recovery.

Yeast expression

Fission yeast strain LD328 was used in this study and general methods to transform into fission yeast cells were as described by Gietz (Gietz, 2014). Briefly, the plasmids were linearized with *NotI* restriction enzyme. Yeast cells were cultured by YES medium at 30°C, 200 rpm until OD_{600} to 0.4-0.8, harvested the cells by centrifugation and washed three times with sterile water. Added Transformation Mix (240 µL 50% PEG3350, 36 µL 1.0 M LiAc, 50 µL single-stranded carrier DNA (2.0 mg/mL) to 34 µl linearized plasmid DNA, resuspended the cells by vortex mixing vigorously and incubated in a 42°C water bath for 40 min. Transformants were plated on EMM+HT (EMM medium supplemented with 45mg/L histidine and 15 µM thiamine) medium. After 3 days, colonies were transferred to EMM+H (EMM medium supplemented with 45mg/L histidine) plates and observed by Zeiss LSM880 confocal laser microscope using a 100× objective.

***In vitro* protein expression and purification**

All proteins were expressed in Escherichia coli BL21 (DE3) cells. Briefly, the protein expression was induced by 0.5 mM isopropyl β-D-1-thiogalactopyranoside (IPTG) for 18 h at 18℃. Cells were collected by centrifugation and lysed with buffer A (40 mM Tris-HCl pH7.4, 500 mM NaCl, 10% glycerol). The bacteria were lysed by sonication and the supernatant was flowed through a column packed with Ni-NTA. Proteins were eluted with buffer B (40 mM Tris-HCl pH7.4, 500 mM NaCl, 500 mM Imidazole) and purified with a Superdex 200 increase 10/300 column (SD200) (GE healthcare). Proteins were stored in buffer C (40 mM Tris-HCl pH7.4, 500 mM NaCl, 1 mM DTT) at -80°C.

For the phase separation experiments *in vitro*, MBP-EH1(FL)-GFP, MBP-EH1(1-684)-GFP and MBP-EH1(1-527)-GFP was cleaved with TEV protease for 3 hours to remove MBP tag. Proteins were diluted to the desired concentrations in different concentration of NaCl. Droplets in 384-well plate were observed by Zeiss LSM880 confocal laser microscope using a ×63 objective.

For the co-localization experiments *in vitro*, 5 µM EH1(FL)-GFP after MBP cleaved and 5 µM mCherry-TOL6 were mixed with buffer (40 mM Tris-HCl pH7.4, 100 mM NaCl) and incubated on ice for 30 min. Droplets in 384-well plate were observed as described previously. GFP was excited at 488 nm and detected at 491-535 nm, mCherry was excited at 561 nm and detected at 579-650 nm.

Pollen tube transformation and imaging

Experiments were performed step by step according to the protocol described in (Noack et al. 2019). Transformed tobacco (*Nicotiana tabacum*) pollen grains were observed 6 hours after transformation with a Zeiss LSM900 laser scanning microscope (Axio Observer 7, inverted) with Airyscan 2 multiplex 4Y mode. 40x Plan Apochromat objective (WI, NA = 1.2) was used during image acquisition. The fluorescence signal was collected with a high-resolution Airyscan2 detector, and ZEN blue software smart set up configured the light paths for TagYFP and mCherry. mCherry smart set-up was used for RFP signal collection due to a lower noise to signal ratio. Laser and camera settings were constant for the entire experiment. Time-lapse of tobacco pollen tubes was acquired between 30-90s. Analysis was performed in FIJI (https://imagej.net/software/fiji/). Region of Interest (ROI) was selected with the "Segmented line" tool over the plasma membrane region of the middle section of the pollen tube for each time point and saved in the ROI manager. An offset distance value was manually calculated for each time point to align each time point to the centre of the pollen tube tip.

Bioinformatics

Prediction of disordered residues (MobiDB consensus scores) and structured residues (Alphafold-plddt) were obtained for individual proteins via MobiDB (https://mobidb.bio.unipd.it). Prediction of prion-like residues were obtained from PLAAC (http://plaac.wi.mit.edu/) using a core length of 60 and 'relative weighting of background probabilities' of 100. Proteome of prion-like domains from *A. thaliana* was obtained from previous work (Chakrabortee et al., 2016; Powers et al., 2019). MobiDB consensus disorder predictions for the *A. thaliana* proteome (NCBI taxon ID 3702) was downloaded on 2021-08-31.

Statistical analysis

For statistical analysis, the R package in R studio was used, and Graphpad Prism.

Multiple sequence alignment and phylogenetic analysis

To identify AtEH1/Pan1 homologues, predicted proteins of selected genomes from the Phytozome v13 database (https://phytozome-next.jgi.doe.gov/blast-search) were searched using the BLASTP algorithm (Altschul*,* S. F. *et al.* 1997) with Arabidopsis AtEH1/Pan1 as an input sequence. Multiple sequence alignment was constructed with the MAFFT algorithm in the einsi mode (Katoh et al., 2017). Phylogenetic analysis was carried out utilizing PhyML v3.0 (Guindon, S. et al., 2010) with the smart model selection (Lefort et al., 2017). The phylogenetic tree was visualized using iTOL v6 (Letunic and Bork 2021*)*.

Figures

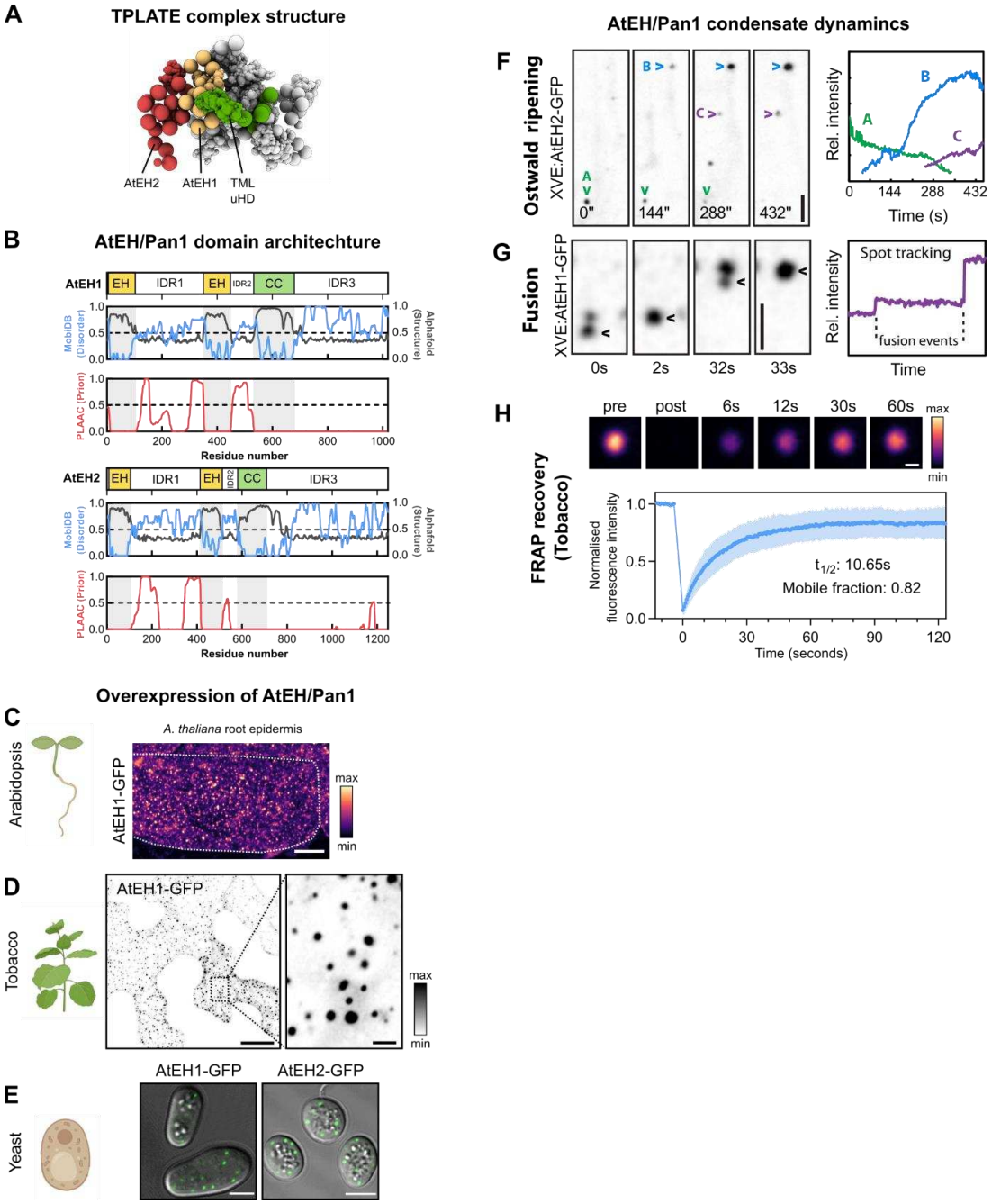

Fig.1. AtEH/Pan1 proteins have the capacity to form liquid-like phase-separated condensates.

A) Integrative Model of the TPLATE complex highlighting AtEH/Pan1 subunits (AtEH1 and AtEH2) and the TML µHD, which connects AtEH1 to the core TPC. PDB: PDBDEV_00000065 (Yperman et al., 2021). B) AtEH1/Pan1 and AtEH2/Pan1 structure and prediction of disordered (MobiDB consensus), structured (Alphafold pLDDT) and prion-like (PLAAC) residues. Values over the 0.5 cutoff are considered disordered, structured, or prion-like respectively. C-E) Airyscan confocal imageof AtEH1 overexpressed in overexpressed in *A. thaliana* root epidermal cells (35S::AtEH1-GFP) (C), *N. benthamiana* epidermal cells (UBQ10:AtEH1-mGFP) (D) and in yeast (*S. pombe*) (E). F-G) Time-lapse imaging of estradiol induced AtEH1 and AtEH2 expression in *A. thaliana* root epidermal cells. Spot tracking and quantification of relative fluorescence intensity shows spot growth and shrinking through ostwald ripening (F), and fusion of spots (G). H) Fluorescence recovery after photobleaching (FRAP) of condensates in *N. benthamiana* epidermal cells transiently expressing UBQ10::AtEH1/Pan1-GFP. Cells were treated with Latrunculin B (4 µM, 30 minutes) to inhibit their movement. Data represents mean ± SD, n= 20 spots from 12 cells. Scale bars = 20µm (D,I), 5µm (C, E, F, G), 2µm (D-inset), 1µm (H).

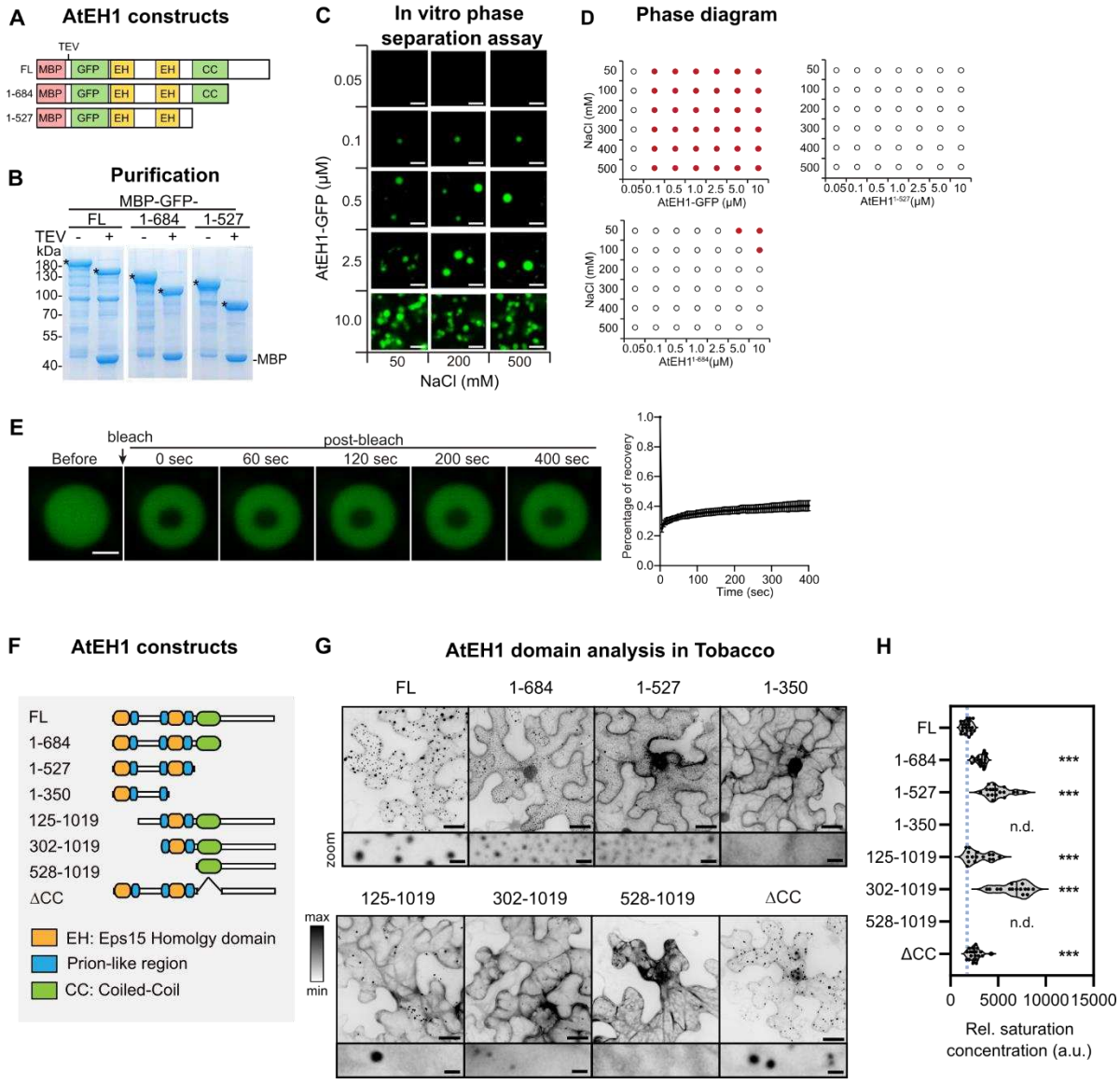

Fig.2. Phase separation capacity of AtEH1/Pan1 is associated with the N-terminally located EH domains and the intrinsically disordered region.

A) Schematic of AtEH1/Pan1 constructs used for protein purification. Constructs were purified as Green Fluorescent protein (GFP)-fusion proteins using an N-terminally located Maltose Binding Protein (MBP) tag with a Tobacco Etch Virus (TEV) cleavage site. EH = EH domain; CC = coiled coil domain. Schematic representation not drawn to scale. B) SDS-PAGE gel of purified AtEH1/Pan1 protein before and after TEV cleavage; * indicates AtEH1/Pan1 protein. C) Concentration dependent, but NaCl independent phase separation of recombinant AtEH1/Pan1 *in vitro.* D) Phase diagram showing the presence of phase separation (red closed circle) under different NaCl and protein concentrations. E) In vitro FRAP assay of purified GFP-$AtEH1_{FL}$ protein. F) Schematic of AtEH1/Pan1 truncation constructs used to analyse the necessary regions for phase separation *in planta*. G) Localisation of AtEH1 truncation constructs (UBQ10:$AtEH1_{domain}$-GFP) transiently expressed in *N. benthamiana*. Insets show zoom in of condensates (dense phase) and cytosol (dilute phase). As the ability of AtEH1/Pan1 to phase separate decreases, protein concentration in the dilute phase increases (increase in cytosolic signal). H) Quantification of relative saturation concentrations obtained by plotting the cytosolic signal intensity. n > 15 cells, *** $p < 0.01$ compared to $AtEH1_{FL}$ from Student's *t*-test. n.d.; not determined (no phase separation). Scale bars 20µm (F), 2 µm (F-inset).

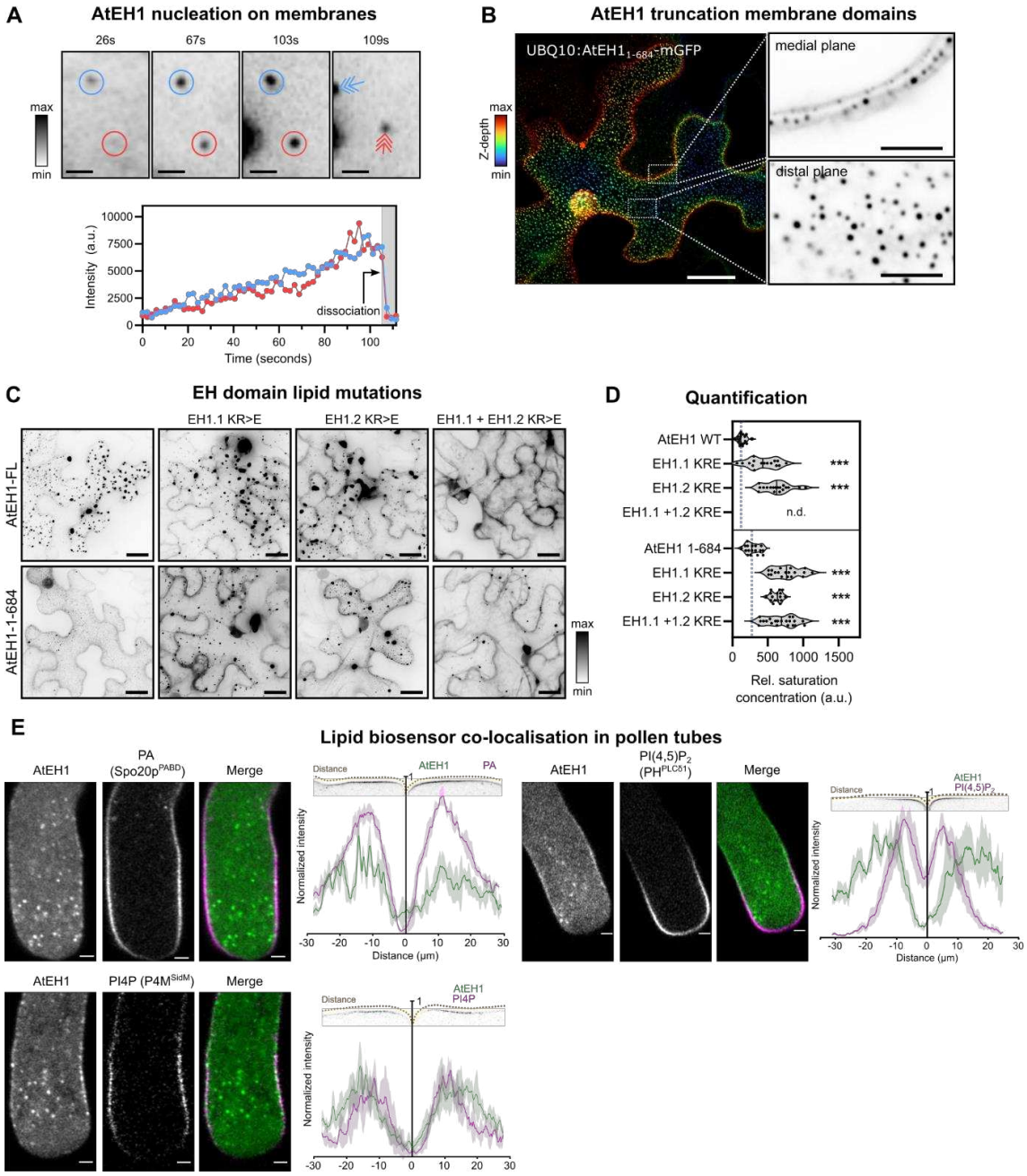

Fig. 3. AtEH/Pan1 condensates nucleate on the plasma membrane.

A) Time-lapse imaging of UBQ10::AtEH1/Pan1-GFP transiently expressed in *N. benthamiana* epidermal cells showing nucleation of condensates on the plasma membrane. Spots appear as immobile dots which gradually increase in intensity, before moving away from the membrane after approx. 110 seconds (arrows). Images represent a Z-projection. B) Depth-coded colour projection of UBQ10:AtEH1$_{1\text{-}684}$-mGFP in *N. benthamiana*. Inset (single Z-plane) shows condensates restricted to a region on the plasma membrane. C) Analysis of EH domain lipid binding mutants in AtEH1 full length and truncated reporters. Mutation of individual lipid binding domains (EH1 KR>E or EH2 R>E) altered condensate distribution and properties. Mutation of both EH domains (EH1 KR>E + EH2 R>E) abolished condensate formation for the AtEH1/Pan1 full length protein, whereas some condensates could form when the construct lacked its C-terminal IDR (AtEH1$_{1\text{-}684}$). D) Quantification of relative saturation concentration. n > 15 cells, *** p < 0.01 Student's *t*-test. n.d; not determined (no phase separation). E) Transient co-expression of pLAT52::AtEH1/Pan1-YFP with lipid biosensors (pLAT52-biosensor-mCherry) in *N. tabacum* pollen tubes. Plasma membrane signal was quantified for AtEH1/Pan1 and lipid biosensors. Two pollen tubes with five different time points were used to quantify the signal at the plasma membrane for each biosensor and AtEH1/Pan1. Data represent a moving average (with a sliding window of 20) with a standard deviation shown in the transparent colour. Scale bars: 20µm (B, C), 5µm (B-inset), 2µm (A, E).

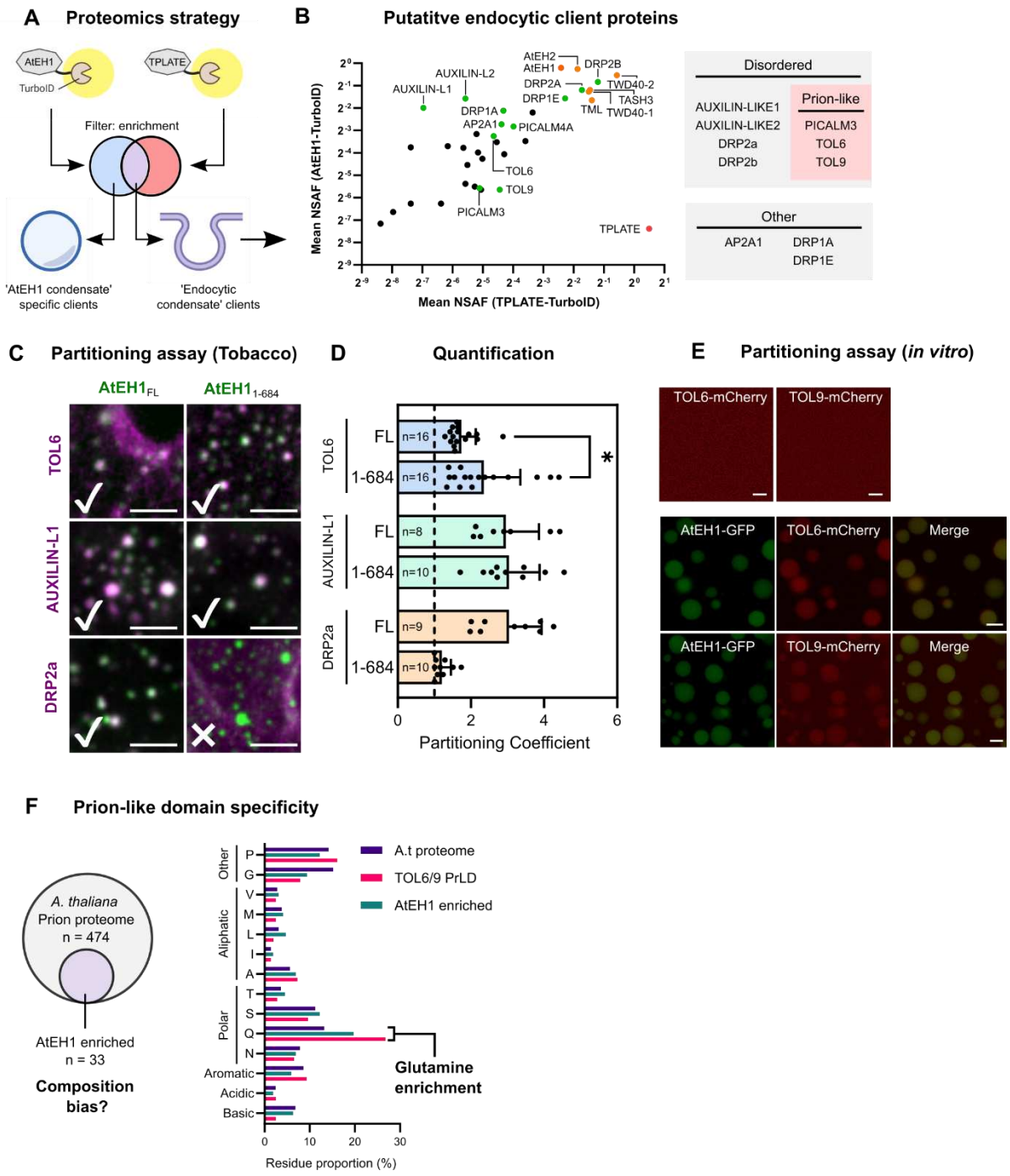

Fig. 4. AtEH/Pan1 proteins recruit endocytic machinery into condensates.

A) Schematic representation of the proteomics strategy to identify client proteins of AtEH1 during endocytosis. B) Plot of common endocytic proteins identified in AtEH1/Pan1-TurboID and TPLATE-TurboID. Colours indicate the following: Endocytic proteins (Green), TPC subunits (Orange), bait (Red). NSAF; normalised spectral abundance factor. Selected proteins were classified based on protein disorder and prion-like domains (shown in Fig S4A-B). C) Partitioning assay using scaffolds (UBQ10::AtEH1(FL)-GFP and UBQ10::AtEH1(1-684)-GFP) and client (UBQ10::Client-mScarlet) transiently in *N. benthamiana* epidermal cells. D) Quantification of client partitioning. A partitioning coefficient of 1 indicates a complete lack of partitioning. *; $p < 0.05$, Student's *t*-test. E) TOL6 and TOL9 partition into AtEH1/Pan1 condensates *in vitro*, but do not phase separate when expressed alone. F) Analysis of enriched residues in prion-like domains from the AtEH1/Pan1-TurboID dataset and TOL6/TOL9 prion-like domains, compared to all prion-like domains from the *A. thaliana* proteome. Glutamine residues are enriched in both TOL6/9 and AtEH1/Pan1-TurboID sets. Scale bars = 2µm (C), 5µm (E).

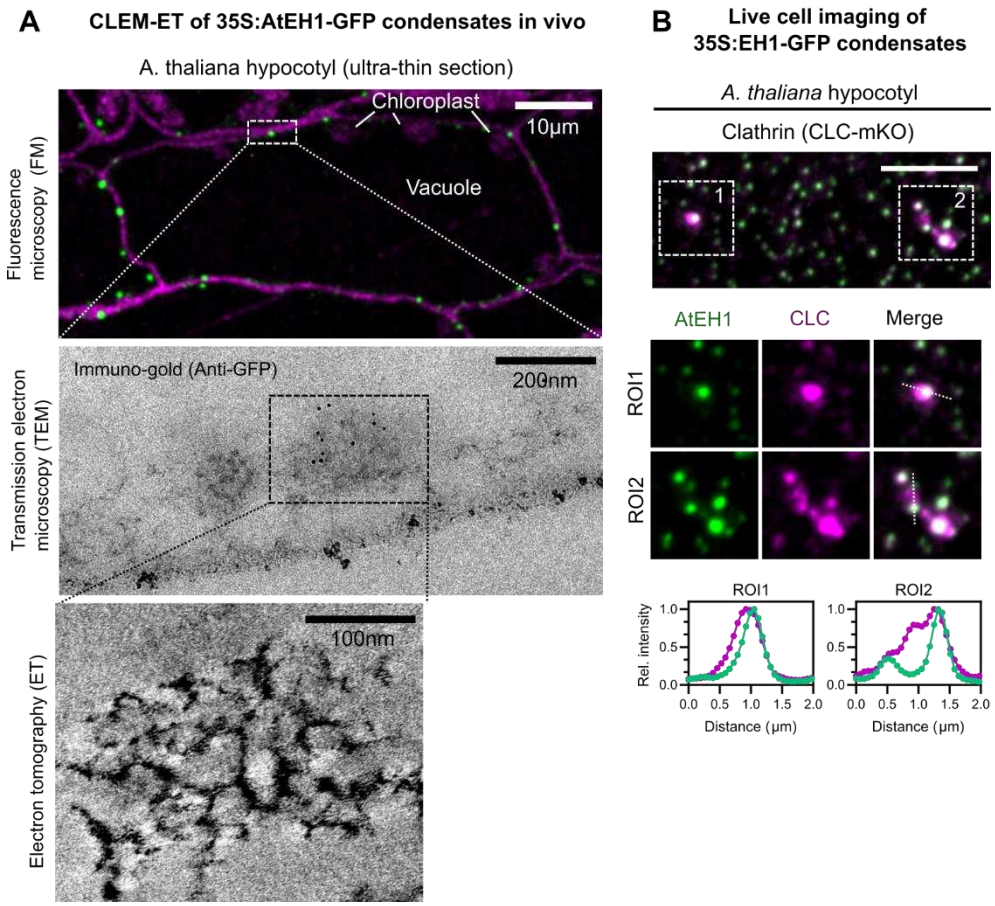

Fig. 5. AtEH1/Pan1 condensates form a platform for clathrin lattice polymerization.

A) Correlative light and electron microscopy (CLEM) combined with Electron Tomography (ET) of hypocotyl sections from stable *A. thaliana* seedlings over-expressing AtEH1/Pan1-GFP. Fluorescence from ultra-thin sections was visualised by fluorescence microscopy (FM) to identify large condensates, which were further confirmed by Anti-GFP immunogold labelling. ET reveals distinctive lattice assemblies strikingly resembling clathrin associated with AtEH1/Pan1 condensates. B) Airyscan confocal images of clathrin light chain 2 (CLC) and AtEH1/Pan1 in *A. thaliana* hypocotyl cells. Plot profiles show normalised fluorescence intensities. Clathrin is observed both within and surrounding the condensates. Scale bars = 5 µm (B)

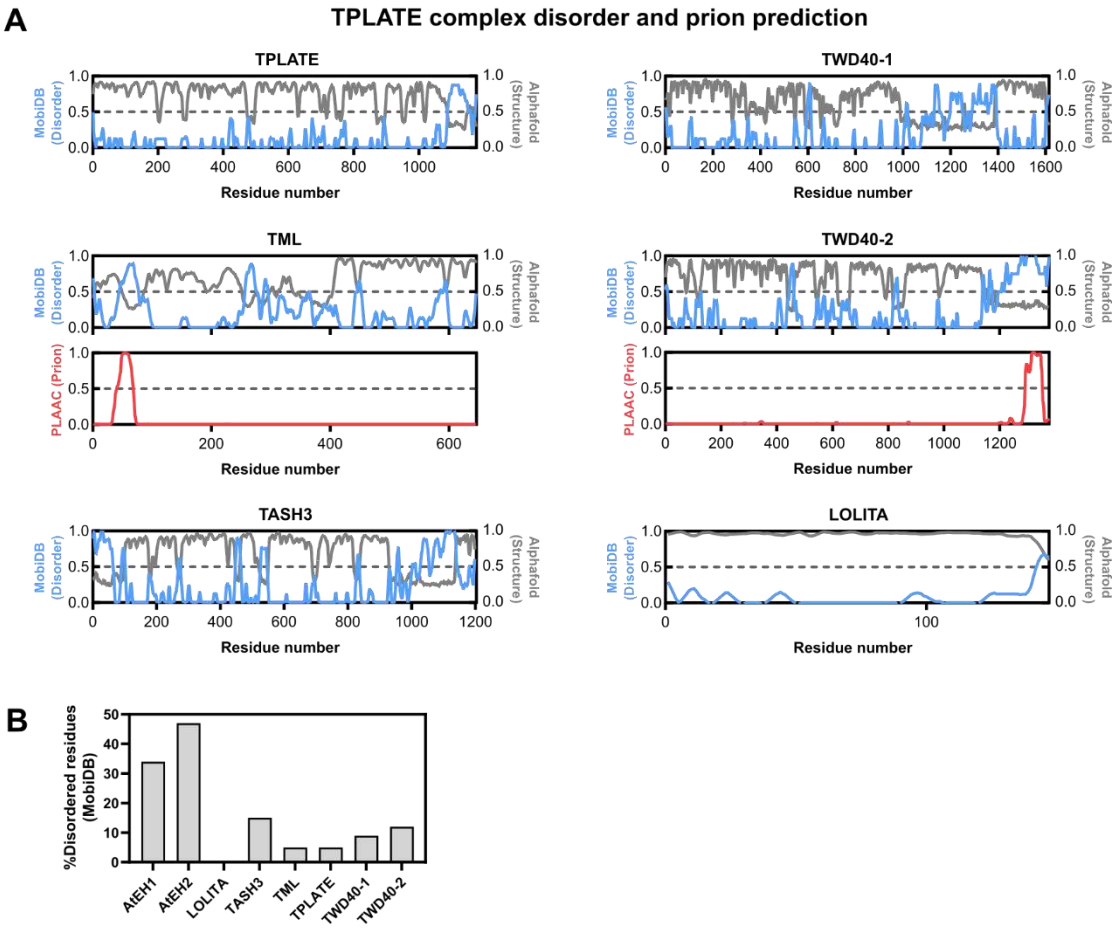

Fig.S1. AtEH/Pan1 proteins are the most disordered TPC subunits.

A) Plot of TPLATE complex subunits showing prediction of disordered (MobiDB consensus, blue), structured (Alphafold2 pLDDT, grey) and prion-like (PLAAC, red) residues. Values over the 0.5 cutoff are considered disordered, structured, or prion-like respectively. B) Plot of the proportion of disordered residues for TPLATE complex subunits. AtEH1/Pan1 and AtEH2/Pan1 are predicted to be highly disordered.

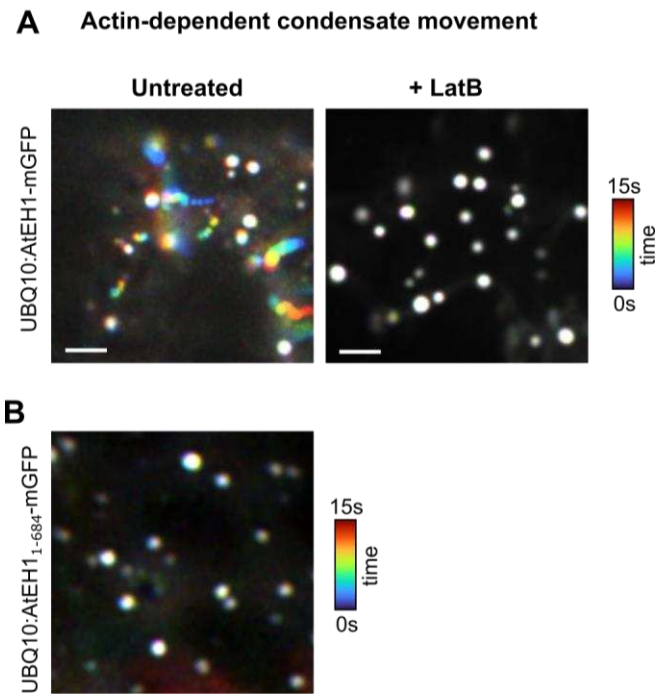

Fig. S2. Condensate mobility can be chemically arrested by inhibiting actin polymerization.

A) Time-lapse projection (time coloured) of *N benthamiana* epidermal cells transiently transfected with UBQ10::AtEH1/Pan1-GFP. Condensates are motile, but become immobile after Latrunculin B treatment (4 µM, 30 minutes). B) Time-lapse imaging showing that UBQ10::AtEH1$_{1-684}$-mGFP condensates are immobile. Scale bars = 5µm.

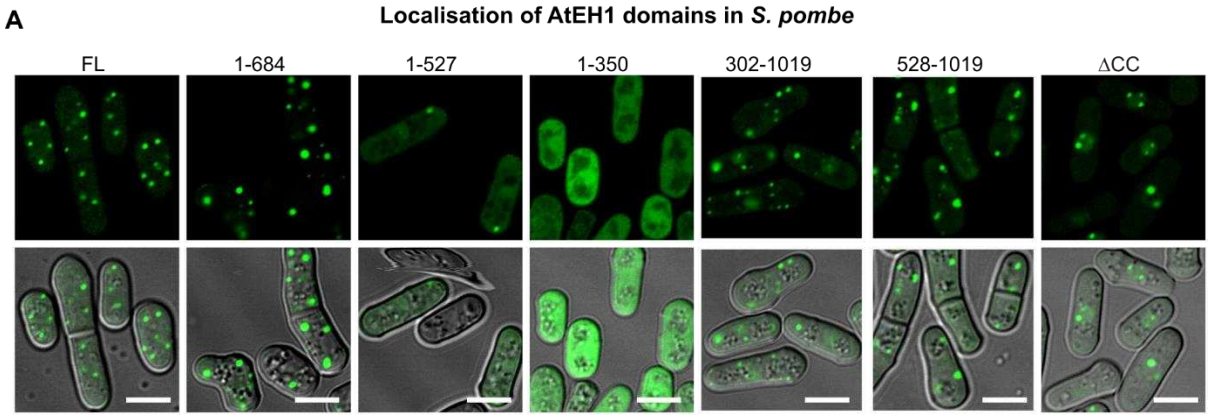

Fig. S3. Various AtEH1/Pan1 truncations form condensates in yeast.

A) Expression and condensate formation capacities of AtEH1/Pan1 domain constructs in *S. pombe*. Scale bars = 2µm. Numbers on top of the panels refer to the length of the constructs used (see Figure 2F).

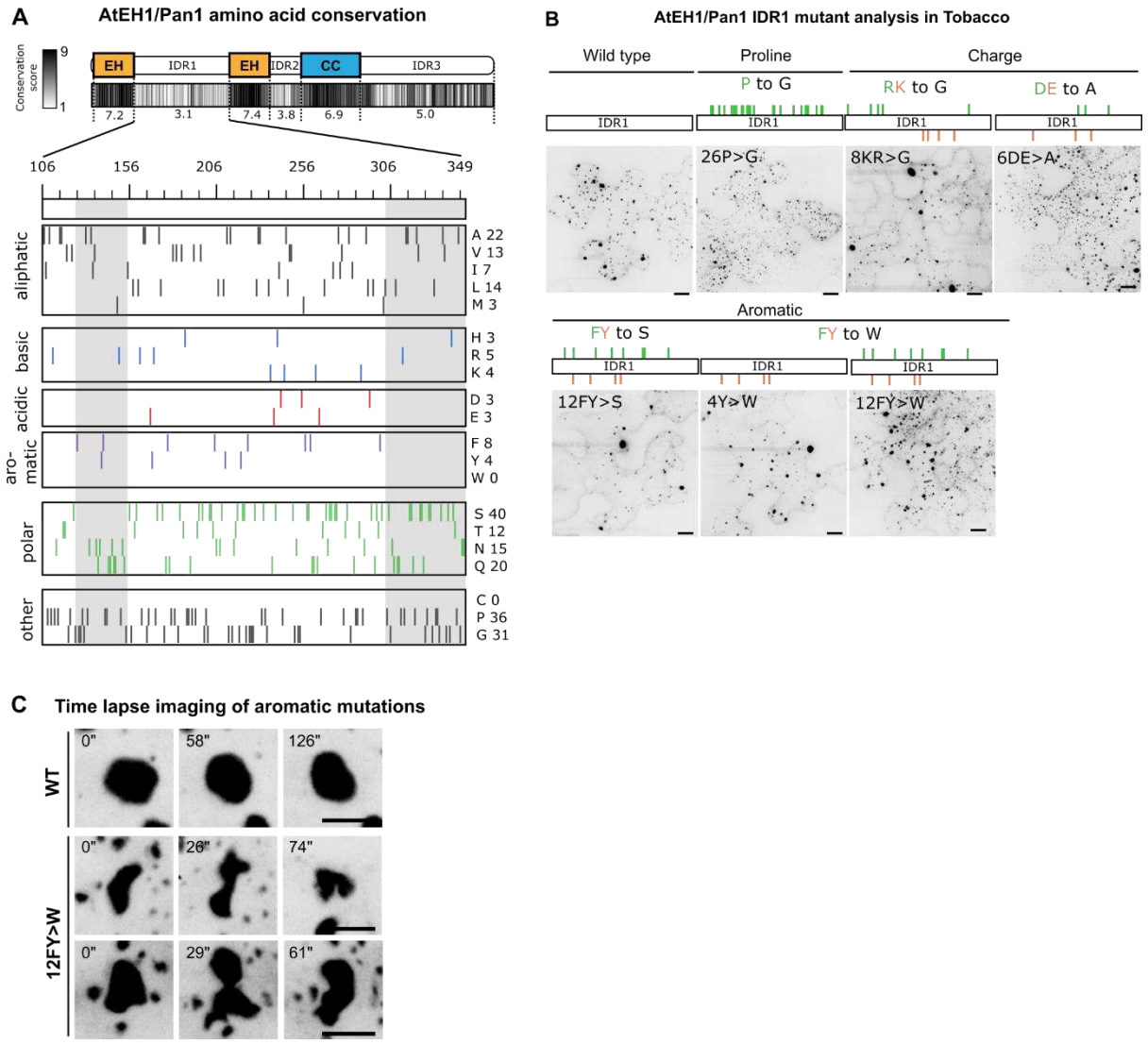

Fig S4. AtEH1/Pan1 IDR1 modulates condensate properties.

A) Conservation of amino acids at the single residue level based on Consurf analysis calculated using 128 AtEH homologous sequences throughout plant evolution. The average conservation score is indicated for each region (1 = 0% conservation, 9 = 100% conservation). IDR1 is highly variable at the individual amino acid level. The composition of IDR1 for AtEH1/Pan1 is shown with each amino acid plotted with total number of each residue indicated. B) Analysis of AtEH1/Pan1 IDR1 mutants transiently expressed in *N. benthamiana* epidermal cells (UBQ10::AtEH1$_{IDR1mut}$-GFP). Mutation of prolines, charged, or aromatic residues changes the properties of the condensates, but did not abolish phase separation capacity. C) Increasing aromatic interaction strength (Y or F to W mutation) lead to condensates which have behaviour of condensates with increased solidity. Condensates were tracked over time (indicated in the top left corner). Scale bars = 5µm (C), 20µm (B).

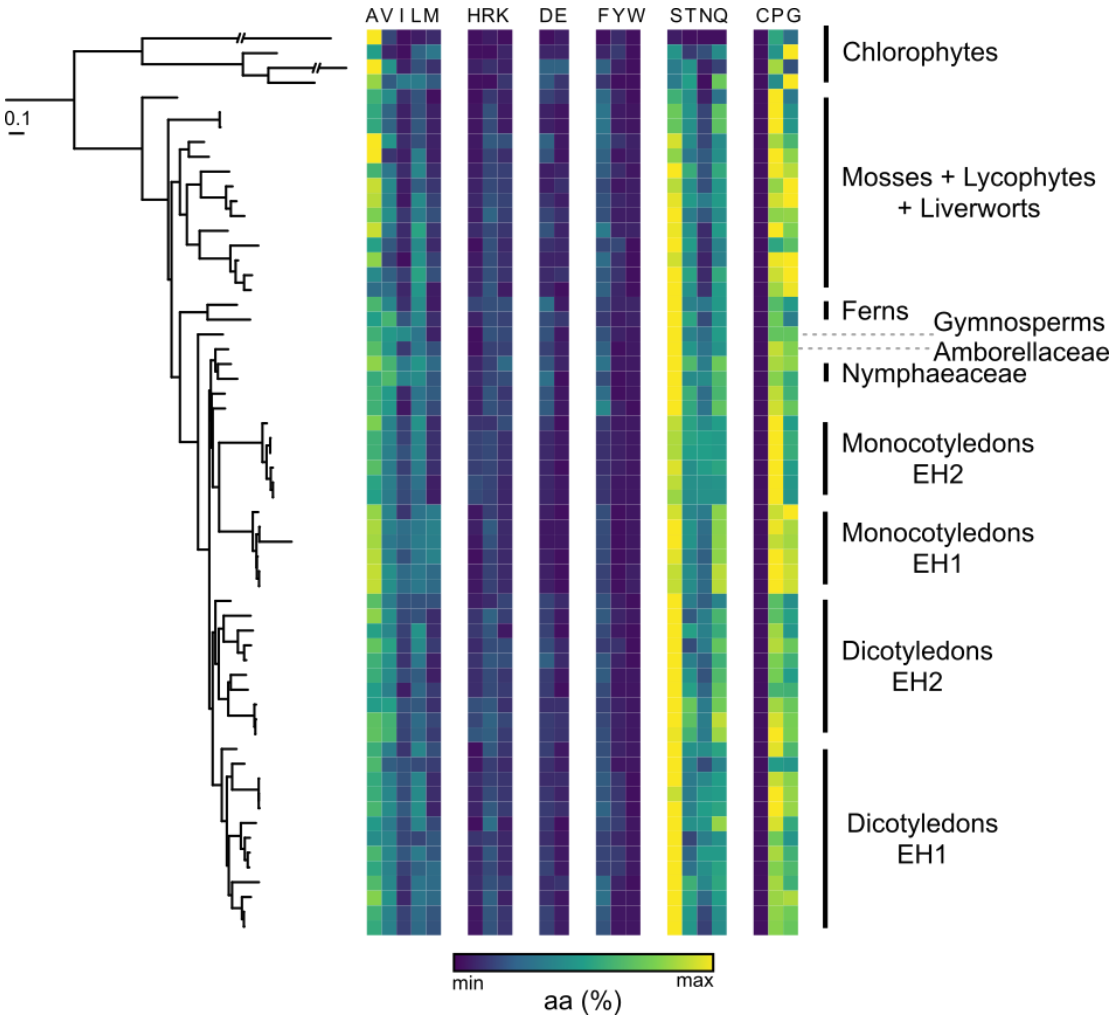

Fig. S5. Evolutionary comparison of AtEH1/Pan1 IDR1 amino acid composition across Archaeplastida.

A tree represents the maximum likelihood phylogeny of EH proteins. The phylogenetic tree was arbitrarily rooted to reflect phylogenetic relationships between chlorophytes lineages and streptophytes.

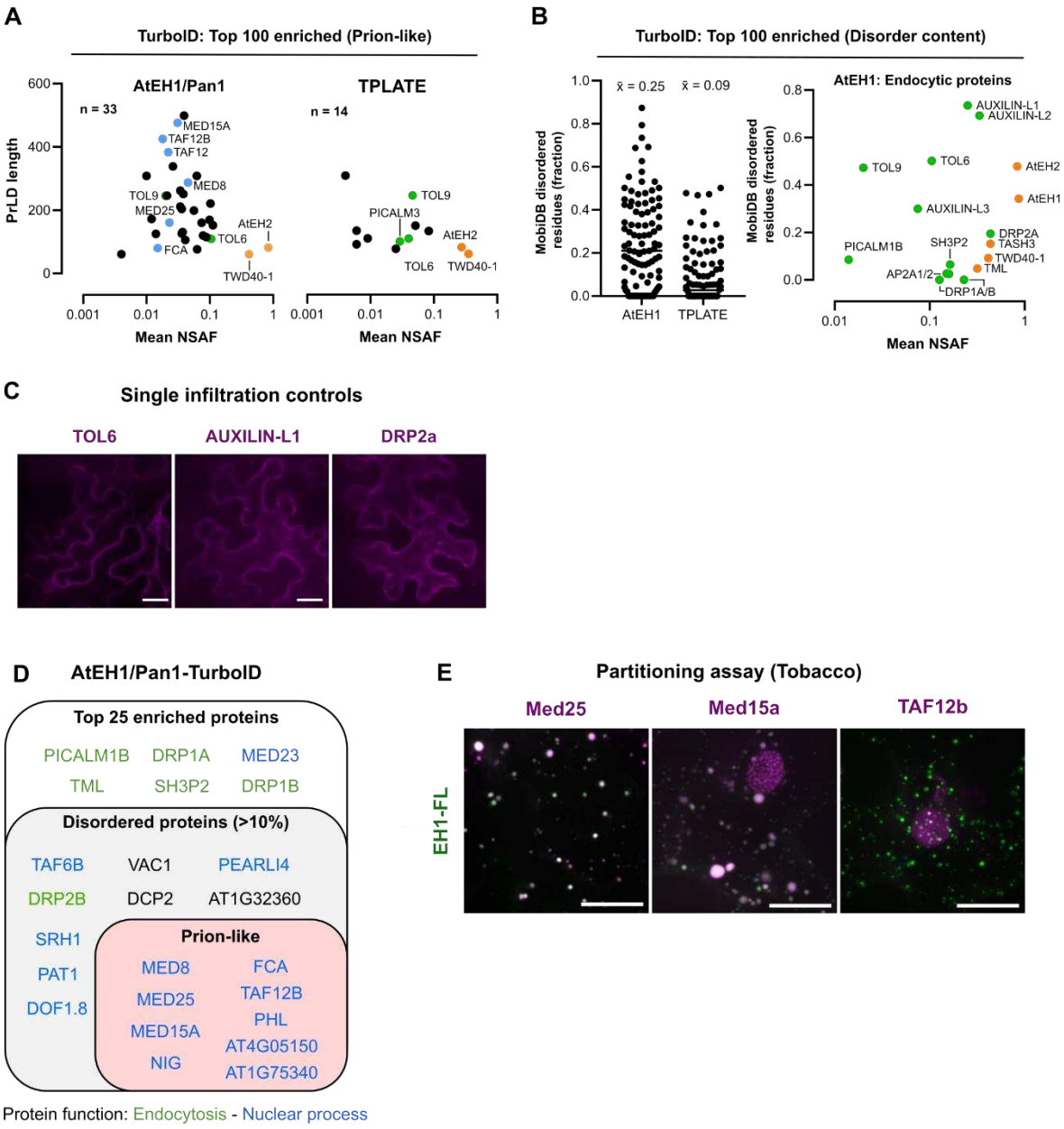

Fig. S6. Compared to the interactome of TPLATE, the AtEH1/Pan1 interactome is enriched for proteins with prion-like domains.

A) Plot of Prion-like proteins identified in the AtEH1/Pan1 and TPLATE TurboID datasets. B) Plot of proteins based on disorder content (MobiDB consensus fraction) and plot showing enrichment versus disorder content of selected individual endocytic proteins. C) Single infiltration controls of AtEH1 clients transiently expressed in *N. benthamiana*. D) Structural categorisation of the top 25 enriched proteins in the AtEH1/Pan1-TurboID dataset. E) Partitioning assay of selected nuclear proteins with prion-like domains identified in the AtEH1/Pan1-TurboID dataset. Scale bars = 20 µm (C, E).

Bibliography

Adamowski, M., Narasimhan, M., Kania, U., Glanc, M., De Jaeger, G. and Friml, J. (2018). A functional study of AUXILIN-LIKE1 and 2, two putative clathrin uncoating factors in arabidopsis. *Plant Cell* **30**, 700–716.

Alaoui, F. El, Casuso, I., Sanchez-Fuentes, D., Arpin-Andre, C., Rathar, R., Baecker, V., Castro, A., Lorca, T., Viaud, J., Vassilopoulos, S., et al. (2022). Structural organization and dynamics of FCHo2 docking on membranes. *Elife* **11**, 1–19.

Alberti, S., Gladfelter, A. and Mittag, T. (2019). Considerations and Challenges in Studying Liquid-Liquid Phase Separation and Biomolecular Condensates. *Cell* **176**, 419–434.

Arora, D., Abel, N. B., Liu, C., Van Damme, P., Yperman, K., Eeckhout, D., Vu, L. D., Wang, J., Tornkvist, A., Impens, F., et al. (2020). Establishment of Proximity-dependent Biotinylation Approaches in Different Plant Model Systems. *Plant Cell* **32**, tpc.00235.2020.

Avinoam, O., Schorb, M., Beese, C. J., Briggs, J. A. G. and Kaksonen, M. (2015). Endocytic sites mature by continuous bending and remodeling of the clathrin coat. *Science (80-.).* **348**, 1369–1372.

Bache, K. G., Raiborg, C., Mehlum, A. and Stenmark, H. (2003). STAM and Hrs are subunits of a multivalent ubiquitin-binding complex on early endosomes. *J. Biol. Chem.* **278**, 12513–12521.

Banani, S. F., Rice, A. M., Peeples, W. B., Lin, Y., Jain, S., Parker, R. and Rosen, M. K. (2016). Compositional Control of Phase-Separated Cellular Bodies. *Cell* **166**, 651–663.

Banani, S. F., Lee, H. O., Hyman, A. A. and Rosen, M. K. (2017). Biomolecular condensates: Organizers of cellular biochemistry. *Nat. Rev. Mol. Cell Biol.* **18**, 285–298.

Bergeron-Sandoval, L. P., Kumar, S., Heris, H. K., Chang, C. L. A., Cornell, C. E., Keller, S. L., François, P., Hendricks, A. G., Ehrlicher, A. J., Pappu, R. V, et al. (2021). Endocytic proteins with prion-like domains form viscoelastic condensates that enable membrane remodeling. *Proc. Natl. Acad. Sci. U. S. A.* **118**, 145664.

Beutel, O., Maraspini, R., Pombo-García, K., Martin-Lemaitre, C. and Honigmann, A. (2019). Phase Separation of Zonula Occludens Proteins Drives Formation of Tight Junctions. *Cell* **179**, 923-936.e11.

Bhave, M., Mino, R. E., Wang, X., Lee, J., Grossman, H. M., Lakoduk, A. M., Danuser, G., Schmid, S. L. and Mettlen, M. (2020). Functional characterization of 67 endocytic accessory proteins using multiparametric quantitative analysis of CCP dynamics. *Proc. Natl. Acad. Sci.* 202020346.

Blanc, C., Charette, S. J., Mattei, S., Aubry, L., Smith, E. W., Cosson, P. and Letourneur, F. (2009). Dictyostelium Tom1 participates to an ancestral ESCRT-0 complex. *Traffic* **10**, 161–171.

Boeke, D., Trautmann, S., Meurer, M., Wachsmuth, M., Godlee, C., Knop, M. and Kaksonen, M. (2014). Quantification of cytosolic interactions identifies E de1 oligomers as key organizers of endocytosis . *Mol. Syst. Biol.* **10**, 756.

Boeynaems, S., Alberti, S., Fawzi, N. L., Mittag, T., Polymenidou, M., Rousseau, F., Schymkowitz, J., Shorter, J., Wolozin, B., Van Den Bosch, L., et al. (2018). Protein Phase Separation: A New Phase in Cell Biology. *Trends Cell Biol.* **28**, 420–435.

Chakrabortee, S., Kayatekin, C., Newby, G. A., Mendillo, M. L., Lancaster, A. and Lindquist, S. (2016). Luminidependens (LD) is an Arabidopsis protein with prion behavior. *Proc. Natl. Acad. Sci. U. S. A.* **113**, 6065–6070.

Chambaud, C., Cookson, S. J., Ollat, N., Bayer, E. and Brocard, L. (2022). A correlative light electron microscopy approach reveals plasmodesmata ultrastructure at the graft interface. *Plant Physiol.* **188**, 44–55.

Cho, W. K., Spille, J. H., Hecht, M., Lee, C., Li, C., Grube, V. and Cisse, I. I. (2018). Mediator and RNA polymerase II clusters associate in transcription-dependent condensates. *Science (80-.).* **361**, 412–415.

Choi, J.-M., Holehouse, A. S. and Pappu, R. V. (2020). Physical Principles Underlying the Complex Biology of Intracellular Phase Transitions. *Annu. Rev. Biophys.* **49**, 107–133.

Cocucci, E., Aguet, F., Boulant, S. and Kirchhausen, T. (2012). The first five seconds in the life of a clathrin-coated pit. *Cell* **150**, 495–507.

Day, K. J., Kago, G., Wang, L., Richter, J. B., Hayden, C. C., Lafer, E. M. and Stachowiak, J. C. (2021). Liquid-like protein interactions catalyse assembly of endocytic vesicles. *Nat. Cell Biol.* **23**, 366–376.

Ditlev, J. A., Case, L. B. and Rosen, M. K. (2018). Who's In and Who's Out—Compositional Control of Biomolecular Condensates. *J. Mol. Biol.* **430**, 4666–4684.

Fang, X., Wang, L., Ishikawa, R., Li, Y., Fiedler, M., Liu, F., Calder, G., Rowan, B., Weigel, D., Li, P., et al. (2019). Arabidopsis FLL2 promotes liquid–liquid phase separation of polyadenylation complexes. *Nature* **569**, 265–269.

Field, M. C., Gabernet-Castello, C. and Dacks, J. B. (2007). Reconstructing the evolution of the endocytic system: Insights from genomics and molecular cell biology. *Adv. Exp. Med. Biol.* **607**, 84–96.

Fujimoto, M., Arimura, S. I., Ueda, T., Takanashi, H., Hayashi, Y., Nakano, A. and Tsutsumi, N. (2010). Arabidopsis dynamin-related proteins DRP2B and DRP1A participate together in clathrin-coated vesicle formation during endocytosis. *Proc. Natl. Acad. Sci.* **107**, 6094–6099.

Fujioka, Y., Alam, J. M., Noshiro, D., Mouri, K., Ando, T., Okada, Y., May, A. I., Knorr, R. L., Suzuki, K., Ohsumi, Y., et al. (2020). Phase separation organizes the site of autophagosome formation. *Nature* **578**, 301–305.

Gadeyne, A., Sánchez-Rodríguez, C., Vanneste, S., Di Rubbo, S., Zauber, H., Vanneste, K., Van Leene, J., De Winne, N., Eeckhout, D., Persiau, G., et al. (2014). The TPLATE adaptor complex drives clathrin-mediated endocytosis in plants. *Cell* **156**, 691–704.

Gietz, R. D. (2014). Yeast transformation by the LiAc/SS carrier DNA/PEG method. In *Yeast Genetics*, pp. 1–12. Springer.

Henne, W. M., Boucrot, E., Meinecke, M., Evergren, E., Vallis, Y., Mittal, R. and McMahon, H. T. (2010). FCHo proteins are nucleators of Clathrin-Mediated endocytosis. *Science (80-.).* **328**, 1281–1284.

Herman, E. K., Walker, G., Van Der Giezen, M. and Dacks, J. B. (2011). Multivesicular bodies in the enigmatic amoeboflagellate Breviata anathema and the evolution of ESCRT. *J. Cell Sci.* **124**, 613–621.

Hirst, J., Schlacht, A., Norcott, J. P., Traynor, D., Bloomfield, G., Antrobus, R., Kay, R. R., Dacks, J. B. and Robinson, M. S. (2014). Characterization of TSET, an ancient and widespread membrane trafficking complex. *Elife* **3**, 1–18.

Hollopeter, G., Lange, J. J., Zhang, Y., Vu, T. N., Gu, M., Ailion, M., Lambie, E. J., Slaughter, B. D., Unruh, J. R., Florens, L., et al. (2014). The membrane-associated proteins FCHo and SGIP are allosteric activators of the AP2 clathrin adaptor complex. *Elife* **3**, 1–23.

Ito, E., Fujimoto, M., Ebine, K., Uemura, T., Ueda, T. and Nakano, A. (2012). Dynamic behavior of clathrin in Arabidopsis thaliana unveiled by live imaging. *Plant J.* **69**, 204–216.

Johnson, A., Dahhan, D. A., Gnyliukh, N., Kaufmann, W. A., Zheden, V., Costanzo, T., Mahou, P., Hrtyan, M., Wang, J., Aguilera-Servin, J., et al. (2021). The TPLATE complex mediates membrane bending during plant clathrin–mediated endocytosis. *Proc. Natl. Acad. Sci. U. S. A.* **118**, 2021.04.26.441441.

Kaksonen, M. and Roux, A. (2018). Mechanisms of clathrin-mediated endocytosis. *Nat. Rev. Mol. Cell Biol.* **19**, 313–326.

Konopka, C. A. and Bednarek, S. Y. (2008). Comparison of the dynamics and functional redundancy of the Arabidopsis dynamin-related isoforms DRP1A and DRP1C during plant development. *Plant Physiol.* **147**, 1590–1602.

Korbei, B., Moulinier-Anzola, J., De-Araujo, L., Lucyshyn, D., Retzer, K., Khan, M. A. and Luschnig, C. (2013). Arabidopsis TOL proteins act as gatekeepers for vacuolar sorting of PIN2 plasma membrane protein. *Curr. Biol.* **23**, 2500–2505.

Kozak, M. and Kaksonen, M. (2019). Phase separation of Ede1 promotes the initiation of endocytic

events. *bioRxiv* 861203.

Lampropoulos, A., Sutikovic, Z., Wenzl, C., Maegele, I., Lohmann, J. U. and Forner, J. (2013). GreenGate - A novel, versatile, and efficient cloning system for plant transgenesis. *PLoS One* **8**,.

Langstein-Skora, I., Schmid, A., Emenecker, R. J., Richardson, M. O. G., Götz, M. J., Payer, S. K., Korber, P. and Holehouse, A. S. (2022). Sequence- and chemical specificity define the functional landscape of intrinsically disordered regions. *bioRxiv* 2022.02.10.480018.

Lehmann, M., Lukonin, I., Noé, F., Schmoranzer, J., Clementi, C., Loerke, D. and Haucke, V. (2019). Nanoscale coupling of endocytic pit growth and stability. *Sci. Adv.* **5**, 1–13.

Liu, D., Mari, M., Li, X., Reggiori, F., Ferro-Novick, S. and Novick, P. (2022). ER-phagy requires the assembly of actin at sites of contact between the cortical ER and endocytic pits. *Proc. Natl. Acad. Sci. U. S. A.* **119**, 1–11.

Lu, R. and Drubin, D. G. (2017). Selection and stabilization of endocytic sites by Ede1, a yeast functional homologue of human Eps15. *Mol. Biol. Cell* **28**, 567–575.

Ma, L., Umasankar, P. K., Wrobel, A. G., Lymar, A., McCoy, A. J., Holkar, S. S., Jha, A., Pradhan-Sundd, T., Watkins, S. C., Owen, D. J., et al. (2015). Transient Fcho1/2·Eps15/R·AP-2 Nanoclusters Prime the AP-2 Clathrin Adaptor for Cargo Binding. *Dev. Cell* **37**, 428–443.

Maldonado-Báez, L., Dores, M. R., Perkins, E. M., Drivas, T. G., Hicke, L. and Wendland, B. (2008). Interaction between Epsin/Yap180 adaptors and the scaffolds Ede1/Pan1 is required for endocytosis. *Mol. Biol. Cell* **19**, 2936–2948.

Martin, E. W., Harmon, T. S., Hopkins, J. B., Chakravarthy, S., Incicco, J. J., Schuck, P., Soranno, A. and Mittag, T. (2021). A multi-step nucleation process determines the kinetics of prion-like domain phase separation. *Nat. Commun.* **12**,.

McMahon, H. T. and Boucrot, E. (2011). Molecular mechanism and physiological functions of clathrin-mediated endocytosis. *Nat. Rev. Mol. Cell Biol.* **12**, 517–533.

Mitrea, D. M. and Kriwacki, R. W. (2016). Phase separation in biology; Functional organization of a higher order Short linear motifs - The unexplored frontier of the eukaryotic proteome. *Cell Commun. Signal.* **14**, 1–20.

Morris, K. L., Jones, J. R., Halebian, M., Wu, S., Baker, M., Armache, J. P., Avila Ibarra, A., Sessions, R. B., Cameron, A. D., Cheng, Y., et al. (2019). Cryo-EM of multiple cage architectures reveals a universal mode of clathrin self-assembly. *Nat. Struct. Mol. Biol.* **26**, 890–898.

Moulinier-Anzola, J., Schwihla, M., De-Araújo, L., Artner, C., Jörg, L., Konstantinova, N., Luschnig, C. and Korbei, B. (2020). TOLs Function as Ubiquitin Receptors in the Early Steps of the ESCRT Pathway in Higher Plants. *Mol. Plant* **13**, 717–731.

Narasimhan, M., Johnson, A., Prizak, R., Kaufmann, W. A., Tan, S., Casillas-Pérez, B. and Friml, J. (2020). Evolutionarily unique mechanistic framework of clathrin-mediated endocytosis in plants. *Elife* **9**,.

Nicolas, W., Bayer, E. and Brocard, L. (2018). Electron Tomography to Study the Three-dimensional Structure of Plasmodesmata in Plant Tissues–from High Pressure Freezing Preparation to Ultrathin Section Collection. *Bio-Protocol* **8**, 1–25.

Noack, L. C. and Jaillais, Y. (2017). Precision targeting by phosphoinositides: how PIs direct endomembrane trafficking in plants. *Curr. Opin. Plant Biol.* **40**, 22–33.

Noack, L. C. and Jaillais, Y. (2020). Functions of Anionic Lipids in Plants. *Annu. Rev. Plant Biol.* **71**, 71–102.

Paez Valencia, J., Goodman, K. and Otegui, M. S. (2016). Endocytosis and endosomal trafficking in plants. *Annu. Rev. Plant Biol.* **67**, 309–335.

Pejchar, P., Sekereš, J., Novotný, O., Žárský, V. and Potocký, M. (2020). Functional analysis of phospholipase Dδ family in tobacco pollen tubes. *Plant J.* **103**, 212–226.

Platre, M. P., Noack, L. C., Doumane, M., Bayle, V., Simon, M. L. A., Maneta-Peyret, L., Fouillen, L., Stanislas, T., Armengot, L., Pejchar, P., et al. (2018). A Combinatorial Lipid Code Shapes the Electrostatic Landscape of Plant Endomembranes. *Dev. Cell* **45**, 1–16.

Potocký, M., Pleskot, R., Pejchar, P., Vitale, N., Kost, B. and Žárský, V. (2014a). Live-cell imaging of

phosphatidic acid dynamics in pollen tubes visualized by S po20p-derived biosensor. *New Phytol.* **203**, 483–494.

Potocký, M., Pleskot, R., Pejchar, P., Vitale, N., Kost, B. and Žárský, V. (2014b). Live-cell imaging of phosphatidic acid dynamics in pollen tubes visualized by Spo20p-derived biosensor. *New Phytol.* **203**, 483–494.

Powers, S. K., Holehouse, A. S., Korasick, D. A., Schreiber, K. H., Clark, N. M., Jing, H., Emenecker, R., Han, S., Tycksen, E., Hwang, I., et al. (2019). Nucleo-cytoplasmic Partitioning of ARF Proteins Controls Auxin Responses in Arabidopsis thaliana. *Mol. Cell* **76**, 177-190.e5.

Rapsomaniki, M. A., Kotsantis, P., Symeonidou, I. E., Giakoumakis, N. N., Taraviras, S. and Lygerou, Z. (2012). EasyFRAP: An interactive, easy-to-use tool for qualitative and quantitative analysis of FRAP data. *Bioinformatics* **28**, 1800–1801.

Sánchez-Rodríguez, C., Shi, Y., Kesten, C., Zhang, D., Sancho-Andrés, G., Ivakov, A., Lampugnani, E. R., Sklodowski, K., Fujimoto, M., Nakano, A., et al. (2018). The Cellulose Synthases Are Cargo of the TPLATE Adaptor Complex. *Mol. Plant* **11**, 346–349.

Sanders, D. W., Kedersha, N., Lee, D. S. W., Strom, A. R., Drake, V., Riback, J. A., Bracha, D., Eeftens, J. M., Iwanicki, A., Wang, A., et al. (2020). Competing Protein-RNA Interaction Networks Control Multiphase Intracellular Organization. *Cell* **181**, 306-324.e28.

Schmid, E. M. and McMahon, H. T. (2007). Integrating molecular and network biology to decode endocytosis. *Nature* **448**, 883–888.

Scholz, P., Pejchar, P., Fernkorn, M., Škrabálková, E., Pleskot, R., Blersch, K., Munnik, T., Potocký, M. and Ischebeck, T. (2022). DIACYLGLYCEROL KINASE 5 regulates polar tip growth of tobacco pollen tubes. *New Phytol.* **233**, 2185–2202.

Skruzny, M., Pohl, E., Gnoth, S., Malengo, G. and Sourjik, V. (2020). The protein architecture of the endocytic coat analyzed by FRET microscopy. *Mol. Syst. Biol.* **16**, 1–13.

Snead, W. T. and Gladfelter, A. S. (2019). The Control Centers of Biomolecular Phase Separation: How Membrane Surfaces, PTMs, and Active Processes Regulate Condensation. *Mol. Cell* **76**, 295–305.

Sparkes, I. a, Runions, J., Kearns, A. and Hawes, C. (2006). Rapid, transient expression of fluorescent fusion proteins in tobacco plants and generation of stably transformed plants. *Nat. Protoc.* **1**, 2019–25.

Stephani, M., Picchianti, L., Gajic, A., Beveridge, R., Skarwan, E., Hernandez, V. S. de M., Mohseni, A., Clavel, M., Zeng, Y., Naumann, C., et al. (2020). A cross-kingdom conserved er-phagy receptor maintains endoplasmic reticulum homeostasis during stress. *Elife* **9**, 1–105.

Stimpson, H. E. M., Toret, C. P., Cheng, A. T., Pauly, B. S. and Drubin, D. G. (2009). Early-arriving Syp1p and Ede1p function in endocytic site placement and formation in budding yeast. *Mol. Biol. Cell* **20**, 4640–4651.

Taylor, M. J., Perrais, D. and Merrifield, C. J. (2011). A high precision survey of the molecular dynamics of mammalian clathrin-mediated endocytosis. *PLoS Biol.* **9**,.

Tebar, F., Confalonieri, S., Carter, R. E., Di Fiore, P. P. and Sorkin, A. (1997). Eps15 is constitutively oligomerized due to homophilic interaction of its coiled-coil region. *J. Biol. Chem.* **272**, 15413–15418.

Tinevez, J. Y., Perry, N., Schindelin, J., Hoopes, G. M., Reynolds, G. D., Laplantine, E., Bednarek, S. Y., Shorte, S. L. and Eliceiri, K. W. (2017). TrackMate: An open and extensible platform for single-particle tracking. *Methods* **115**, 80–90.

Van Damme, D., Coutuer, S., De Rycke, R., Bouget, F. Y., Inzé, D. and Geelen, D. (2006). Somatic cytokinesis and pollen maturation in Arabidopsis depend on TPLATE, which has domains similar to coat proteins. *Plant Cell* **18**, 3502–3518.

Van Damme, D., Gadeyne, A., Vanstraelen, M., Inzé, D., Van Montagu, M. C. E., De Jaeger, G., Russinova, E. and Geelen, D. (2011). Adaptin-like protein TPLATE and clathrin recruitment during plant somatic cytokinesis occurs via two distinct pathways. *Proc. Natl. Acad. Sci. U. S. A.* **108**, 615–620.

Wang, P., Pleskot, R., Zang, J., Winkler, J., Wang, J., Yperman, K., Zhang, T., Wang, K., Gong, J., Guan, Y., et al. (2019). Plant AtEH/Pan1 proteins drive autophagosome formation at ER-PM contact sites with actin and endocytic machinery. *Nat. Commun.* **10**, 1–16.

Wang, J., Mylle, E., Johnson, A., Besbrugge, N., De Jaeger, G., Friml, J., Pleskot, R. and Van Damme, D. (2020). High Temporal Resolution Reveals Simultaneous Plasma Membrane Recruitment of TPLATE Complex Subunits. *Plant Physiol.* **183**, 986–997.

Wang, J., Yperman, K., Grones, P., Jiang, Q., Dragwidge, J., Mylle, E., Mor, E., Nolf, J., Eeckhout, D., de Jaeger, G., et al. (2021). Conditional destabilization of the TPLATE complex impairs endocytic internalization. *Proc. Natl. Acad. Sci. U. S. A.* **118**, e2023456118.

Wilfling, F., Lee, C. W., Erdmann, P. S., Zheng, Y., Sherpa, D., Jentsch, S., Pfander, B., Schulman, B. A. and Baumeister, W. (2020). A Selective Autophagy Pathway for Phase-Separated Endocytic Protein Deposits. *Mol. Cell* **80**, 764-778.e7.

Winkler, J., Mylle, E., de Meyer, A., Pavie, B., Merchie, J., Grones, P. and van Damme, D. (2021). Visualizing protein–protein interactions in plants by rapamycin-dependent delocalization. *Plant Cell* **33**, 1101–1117.

Yang, P., Mathieu, C., Kolaitis, R. M., Zhang, P., Messing, J., Yurtsever, U., Yang, Z., Wu, J., Li, Y., Pan, Q., et al. (2020). G3BP1 Is a Tunable Switch that Triggers Phase Separation to Assemble Stress Granules. *Cell* **181**, 325-345.e28.

Yperman, K., Wang, J., Eeckhout, D., Winkler, J., Vu, L. D., Vandorpe, M., Grones, P., Mylle, E., Kraus, M., Merceron, R., et al. (2021a). Molecular architecture of the endocytic TPLATE complex. *Sci. Adv.* **7**,.

Yperman, K., Papageorgiou, A. C., Merceron, R., De Munck, S., Bloch, Y., Eeckhout, D., Jiang, Q., Tack, P., Grigoryan, R., Evangelidis, T., et al. (2021b). Distinct EH domains of the endocytic TPLATE complex confer lipid and protein binding. *Nat. Commun.* **12**,.

Zhang, Y., Persson, S., Hirst, J., Robinson, M. S., van Damme, D. and Sánchez-Rodríguez, C. (2015). Change your Tplate, change your fate: Plant CME and beyond. *Trends Plant Sci.* **20**, 41–48.

Zhao, Y. G. and Zhang, H. (2020). Phase Separation in Membrane Biology: The Interplay between Membrane-Bound Organelles and Membraneless Condensates. *Dev. Cell* 1–15.